
ALTBI: Constructing Improved Outlier Detection Models via Optimization of Inlier-Memorization Effect

Seoyoung Cho¹ Jaesung Hwang² Kwan-Young Bak^{1,3} Dongha Kim^{1,3}

Abstract

Outlier detection (OD) is the task of identifying unusual observations (or outliers) from a given or upcoming data by learning unique patterns of normal observations (or inliers). Recently, a study introduced a powerful unsupervised OD (UOD) solver based on a new observation of deep generative models, called *inlier-memorization (IM) effect*, which suggests that generative models memorize inliers before outliers in early learning stages. In this study, we aim to develop a theoretically principled method to address UOD tasks by *maximally utilizing the IM effect*. We begin by observing that the IM effect is observed more clearly when the given training data contain fewer outliers. This finding indicates a potential for enhancing the IM effect in UOD regimes if we can effectively exclude outliers from mini-batches when designing the loss function. To this end, we introduce two main techniques: 1) increasing the mini-batch size as the model training proceeds and 2) using an adaptive threshold to calculate the truncated loss function. We theoretically show that these two techniques effectively filter out outliers from the truncated loss function, allowing us to utilize the IM effect to the fullest. Coupled with an additional ensemble technique, we propose our method and term it *Adaptive Loss Truncation with Batch Increment (ALTBI)*. We provide extensive experimental results to demonstrate that ALTBI achieves state-of-the-art performance in identifying outliers compared to other recent methods, even with lower computation costs. Additionally, we show that our method yields robust performances when combined with privacy-preserving algorithms.

¹Department of Statistics, Sungshin Women’s University, Seoul, Republic of Korea ²SK Telecom, Seoul, Republic of Korea ³Data Science Center, Sungshin Women’s University, Seoul, Republic of Korea. Correspondence to: Dongha Kim <dongha0718@gmail.com>.

1. Introduction

Outlier detection: Outlier detection (OD) is an important task in various fields, aiming to identify unusual observations, or outliers. This process involves learning the distinct patterns of normal observations, known as inliers, and developing efficient scores to distinguish between inliers and outliers. The ability to accurately detect outliers is essential for ensuring data quality and reliability in applications such as fraud detection, network security, and fault diagnosis.

OD tasks can be divided into three cases depending on availability of anomalousness information of given training data. Supervised OD (SOD) uses labeled data to classify each sample as either outlier or not. Semi-supervised OD (SSOD), also known as out-of-distribution detection, assumes that all training data are normal and builds models based only on these inliers. Unsupervised OD (UOD) works with data that may contain outliers but has no labels to identify them. In UOD tasks, the primary goal is to accurately identify outliers in a given training dataset. In general, many real-world anomaly detection tasks belong to UOD because outliers in large datasets are usually unknown beforehand. Hence, we focus on addressing UOD problems in this study.

Recent advancements in machine learning domains have introduced powerful UOD methods. In particular, many studies have leveraged deep generative models (DGM) to develop unique scores to identify outliers. Surprisingly, conventional likelihood was not utilized, as it has been widely recognized that it often confuses outliers with inliers when the models are fully trained (Nalisnick et al., 2019b;a; Lan & Dinh, 2021).

Recently, a notable study has highlighted the potential of the likelihood values of DGMs in UOD tasks, based on the observation of the *inlier-memorization (IM) effect* (Kim et al., 2024). This effect suggests that when a DGM is trained, the loss values, i.e., the negative log-likelihoods, of inliers decrease before those of outliers in early training stages. This implies that the likelihood value itself can be a favorable measure to identify outliers with *under-fitted DGMs*. Leveraging this phenomenon, Kim et al. (2024) developed a UOD solver called ODIM, which has demonstrated powerful yet computationally efficient performance in identifying inliers

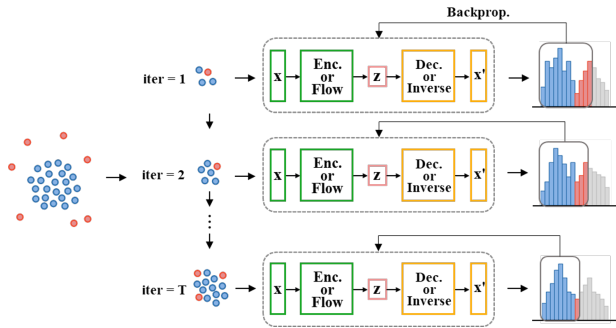


Figure 1. An illustration of ALTBI.

within a dataset.

Improvement of IM effect: Inspired by ODIM, this study aims to develop an enhanced UOD method by maximally exploiting the IM effect. We begin by observing that the clarity of the IM effect becomes more pronounced as the training data contain fewer outliers. We visually illustrate this simple but important finding in Figure 2. This observation suggests that boosting the IM effect could be achieved if we can effectively separate outliers from inliers and exclude them when constructing loss functions during the early training stages.

To this end, we introduce two key techniques: 1) gradually increasing the mini-batch size and 2) adopting an adaptive threshold to truncate the loss function. These techniques are designed to maximize the utility of the IM effect, ensuring more accurate identification of outliers. We provide theoretical results showing that these two techniques result in the ratio of outliers included in the truncated loss function decreasing toward zero as training proceeds.

Additionally, we incorporate an ensemble strategy of loss values within a single DGM with various updates to further enhance our method’s performance and stability. We demonstrate that this simple technique significantly improves the outlier detecting performance without additional computational or resource costs.

Combining all the above elements, we develop a powerful framework for addressing UOD tasks and term it *Adaptive Loss Truncation with Batch Increment (ALTBI)*. We present Figure 1 to visualize our method. Our method has several notable advantages over other existing UOD solvers. First, our method consistently achieves superior results in detecting outliers from a given dataset. Through extensive experiments analyzing 57 datasets, we demonstrate that ALTBI achieves state-of-the-art performance in outlier detection.

Additionally, ALTBI only requires a simple and under-fitted likelihood-based DGM, training with variational autoencoders (VAE, Kingma & Welling (2013)) or normalizing

flows (NF, Dinh et al. (2017)) for up to hundreds of mini-batch updates. This makes ALTBI highly efficient, requiring significantly reduced computational costs compared to other recent methods. Our findings indicate that ALTBI is a promising approach for efficient and effective UOD solution in various practical applications.

The remainder of our paper is organized as follows. We first provide a brief review of related research on OD problems, primarily focusing on SSOD and UOD. Then, we offer detailed descriptions of ALTBI along with its motivations, followed by its theoretical discussions. The results of various experiments are presented, including performance tests, ablation studies, and further discussions related to data privacy. Finally, concluding remarks are provided. The key contributions of our work are:

- We find that the IM effect is observed more apparently when the training data have fewer outliers.
- We develop a theoretically well-grounded and powerful UOD solution called ALTBI, using truncated loss functions with incrementally increasing mini-batch sizes.
- We empirically validate the superiority of ALTBI in detecting outliers by analyzing 57 datasets.

2. Related works

We first review studies dealing with SSOD problems. SVDD (Tax & Duin, 2004) uses kernel functions to construct a boundary around a dataset for outlier detection, while DeepSVDD (Ruff et al., 2018) extends SVDD by using a deep autoencoder to obtain a feature space where normal data lies within a boundary, while anomalies fall outside. DeepSAD (Ruff et al., 2020) generalizes DeepSVDD by considering an extended scenarios where a small amount of labeled outliers are also available.

Self-supervised learning has been widely applied to address SSOD tasks (Tack et al., 2020; Golan & El-Yaniv, 2018). In particular, SimCLR (Chen et al., 2020) leverages the contrastive learning to obtain high-quality feature representations of inliers, and ICL (Shenkar & Wolf, 2022) maximizes mutual information between masked and unmasked parts of data to successfully detect outliers.

Numerous traditional approaches have been proposed to address UOD problems. LOF (Breunig et al., 2000a) detects local outliers in a dataset based on density. This idea has been extended to CBLOF (He et al., 2003), which identifies outliers based on the distance from the nearest cluster and the size of the cluster it belongs to, measuring the significance of an outlier. MCD (Fauconnier & Haesbroeck, 2009) identifies outliers by finding a subset of the data with the smallest covariance determinant, providing powerful outlier

scores using estimates of location and scatter. IF (Liu et al., 2008) detects anomalies by isolating data points using tree structures.

There are also various techniques to solve UOD problems using deep learning models. RDA (Zhou & Paffenroth, 2017) extends deep autoencoder by incorporating robustness against outliers, and DSEBM (Zhai et al., 2016) generates an energy function as the output of a deterministic deep neural network. Additionally, ODIM (Kim et al., 2024) utilizes the inlier-memorization effect observed in the early training updates of deep generative models to identify outliers. DTE (Livernoche et al., 2023) estimates the distribution over diffusion time for a given input and uses the mode or mean of this distribution as the anomaly score.

3. Detailed description of ALTBI

3.1. Preliminaries

Notations and definitions We introduce notations and definitions frequently used throughout this paper. Let $X_1, \dots, X_n (\in \mathcal{X} \subset \mathbb{R}^D) \sim P_*$ be n independent random input vectors following the true distribution P_* . Since training data contain outliers as well as inliers in the UOD regime, we assume that P_* is a mixture of two distributions, i.e., $P_* = (1 - \alpha)P_i + \alpha P_o$, where P_i, P_o represent the inlier and outlier distributions, respectively, and $\alpha \in (0, 1)$ is the outlier ratio. And we define the support of P_i and P_o as \mathcal{X}_i and \mathcal{X}_o , respectively (hence $\mathcal{X} = \mathcal{X}_i \cup \mathcal{X}_o$). Since inliers and outliers do not share their supports, we can obviously assume $\mathcal{X}_i \cap \mathcal{X}_o = \emptyset$.

We denote a training dataset comprising n observations by $\mathcal{D}^{\text{tr}} = \{\mathbf{x}_1, \dots, \mathbf{x}_n\}$. For a given sample \mathbf{x} , a per-sample loss function with a given DGM is defined as $l(\theta; \mathbf{x})$, where $\theta \in \Theta$ represents the parameters for constructing the DGM. Since we consider likelihood-based DGMs such as VAE-based ones (Kingma & Welling, 2013; Burda et al., 2016; Kim et al., 2020), or NF-based ones (Dinh et al., 2015; 2017; Kingma & Dhariwal, 2018), $l(\mathbf{x}; \theta)$ would be the negative log-likelihood (or ELBO). Without loss of generality, we assume that $l(\theta; \mathbf{x})$ is differentiable and bounded by $[0, 1]$ for any $\mathbf{x} \in \mathcal{X}$ and $\theta \in \Theta$.

The risk function calculated over a distribution P is denoted by $L(\theta, P) = E_{X \sim P} [l(\theta; X)]$.

We respectively abbreviate $L(\theta, P_i)$ and $L(\theta, P_o)$ as $L_i(\theta)$ and $L_o(\theta)$. Finally, we denote the minimizer of the inlier risk as θ_* , i.e., $\theta_* = \operatorname{argmin}_{\theta} L_i(\theta)$. We assume $L_i(\theta_*) = 0$.

Brief review of ODIM ODIM (Kim et al., 2024) is a UOD solver that utilizes the IM effect for the first time. The IM effect refers to a phenomenon where, when training a DGM with a given dataset that may contain outliers, the model

eventually learns all the patterns of the data, but there is a gap in the memorization order between inliers and outliers. That is, the model memorizes inliers first during the early updates. Inliers are more prevalent and densely distributed than outliers, thus, reducing the per-sample loss values of inliers first is a more beneficial direction to minimize the overall (averaged) loss function in the early training stages, which might be an intuitive explanation of the IM effect.

ODIM trains likelihood-based DGMs, such as VAE (Kingma & Welling, 2013), for a certain number of updates and uses the per-sample loss values as the outlier score. To find the optimal number of updates where the IM effect is most clearly observed, ODIM examines the degree of bi-modality in the per-sample loss distribution at each update.

To this end, at each update, ODIM fits a 2-cluster Gaussian mixture model to the per-sample loss distribution and calculates the dissimilarity between the two clusters using measures such as the Wasserstein distance. The bi-modality measures are monitored for all updates, and the update with the maximum measure is chosen as the optimal point.

To enhance outlier identification performance, an ensemble technique is also adopted. Multiple under-fitted DGMs are independently trained, and the final score of a given sample \mathbf{x} is calculated as the average per-sample loss value, given as:

$$s^{\text{ODIM}}(\mathbf{x}) = \frac{1}{B} \sum_{b=1}^B l(\theta^{(b)}; \mathbf{x}),$$

where $\theta^{(b)}, b = 1, \dots, B$ are the B estimated parameters from independent initializations. And the sample \mathbf{x} is regarded as an outlier if its score is large, and vice versa.

3.2. Relationship between IM effect and outlier ratio

The IM effect implies that distinguishing inliers from outliers is viable by using the per-sample loss values with an under-fitted DGM. In this section, we claim that the clarity of the IM effect increases as the proportion of outliers in the training dataset decreases. To demonstrate this, we conduct a simple experiment analyzing the PageBlocks dataset with various outlier ratios ranging from 1% to 9%. In each setting, we train a VAE for 100 mini-batch updates with a mini-batch size of 128 and evaluate the AUC values of the training data for identifying outliers using per-sample loss values.

Figure 2 illustrates that the IM effect is observed more clearly as the training data contain fewer outliers, which strongly validates our claim. This observation leads to a new belief: if we can effectively filter out outliers when constructing loss values using a mini-batch to update parameters, we can strengthen the IM effect, thereby enhancing

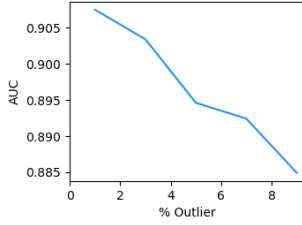


Figure 2. Relationship between the outlier ratio in training data and IM effect.

outlier detection performance. This is the main motivation of our study.

3.3. Proposed method

Mini-batch increment and adaptive threshold We again note that the goal is to maximize the utility of the IM effect in early training updates. To this end, we introduce two simple but powerful strategies to obtain a refined loss function: 1) using a mini-batch size that gradually increases as training proceeds and 2) utilizing a truncated loss function with an adaptive threshold.

To be more specific, as a *warm-up* phase, for given integers n_0 and T_0 , we first train a DGM with a conventional loss function using mini-batches with a fixed size of n_0 for T_0 updates. We use this non-truncated loss function to obtain an estimated parameter where the IM effect starts to appear.

After that, as the second phase, we apply the mini-batch increment and loss truncation strategies. At each update iteration t , we access a mini-batch $\mathcal{D}_t \subset \mathcal{D}^u$ whose size is an exponential function of the iteration t , i.e., $|\mathcal{D}_t| = n_0 \gamma^{t-1} (= n_t)$ for a constant $\gamma > 1$. And instead of using all the samples included in \mathcal{D}_t to calculate the loss function, we exploit the *truncated loss function* which is formularized as:

$$\hat{L}(\theta, \tau_t; \mathcal{D}_t) = \frac{\sum_{\mathbf{x} \in \mathcal{D}_t} l(\theta; \mathbf{x}) \cdot I(l(\theta; \mathbf{x}) \leq \tau_t)}{\sum_{\mathbf{x}' \in \mathcal{D}_t} I(l(\theta; \mathbf{x}') \leq \tau_t)}, \quad (1)$$

where $\tau_t > 0$ is an adaptive threshold.

Theoretically, we set τ_t to be the inlier risk, i.e., $\tau_t = L_i(\theta_{t-1})$, where θ_{t-1} is the estimated parameter at $(t-1)$ -th update with an SGD-based optimizer. However, the computation of $\tau_t = L_i(\theta_{t-1})$ is infeasible in practice since we do not know the anomaly information of the training samples. Instead, we introduce the quantile as the value of τ_t . Specifically, for a pre-specified value $0 < \rho < 1$, we filter out the $100 \times (1 - \rho)\%$ of the samples in the mini-batch that have the largest per-sample loss values.

We conduct a simple experiment to empirically validate the effect of use of mini-batch increment and adaptive threshold. Two VAEs are trained in two scenarios—one with and

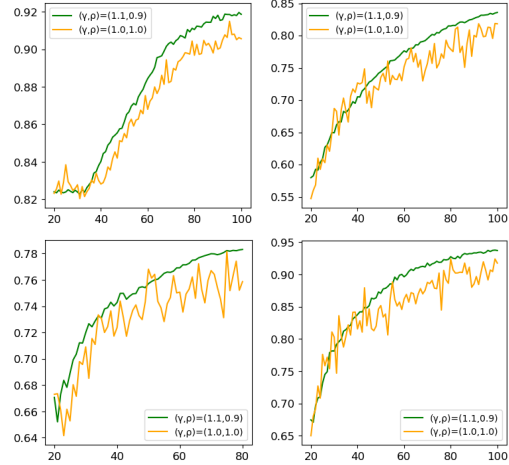


Figure 3. Outlier detection AUC values for DGMs with and without applying mini-batch increment and adaptive threshold, coloured as green and orange, respectively. (Upper left to clockwise) We analyze Ionosphere, Letter, Vowels, and MagicGamma datasets.

the other without applying the two strategies. For the first scenario, we set $(T_0, n_0, \gamma, \rho) = (10, 128, 1.1, 0.9)$. The outlier detection AUC results of the training data over four datasets are illustrated in Figure 3. We can clearly observe that the IM effect is more pronounced when using the two strategies, leading to superior performance in outlier detection. Additionally, using an increasing mini-batch size reduces fluctuation over updates, resulting in a more stable trained model. The theoretical properties of using adaptive mini-batch size and threshold will be discussed in the subsequent section.

Remark 3.1. Increasing the mini-batch size and using truncated loss function during training were first proposed in Xu et al. (2021). They utilized these techniques to develop enhanced classifiers in semi-supervised learning tasks. Our proposed method has its own contribution in that we find the close connection between the IM effect and these two techniques in the UOD regime and apply them to train DGMs with high outlier detection performance.

Ensemble within a single model Recall that ODIM measures the degree of bi-modality in the per-sample loss distribution to find the optimal update. We empirically find that this heuristic approach often fails to identify the optimal update where the IM effect is maximized, sometimes even selecting an update where the IM effect does not appear. Additionally, ODIM employs an ensemble method to enhance performance using multiple under-fitted models, which increases computation time and resources.

To address this issue, we neither measure bi-modality nor use multiple models. Instead, we adopt the ensemble ap-

proach *within a single model*. For given two integers T_1, T_2 with $T_1 < T_2$, we take the average of per-sample loss values from $T_1 + 1$ to T_2 updates. That is, for a given input \mathbf{x} , we compute its outlier score as

$$s^{\text{ALTBI}}(\mathbf{x}) = \frac{1}{T_2 - T_1} \sum_{t=T_1+1}^{T_2} l(\theta_t; \mathbf{x}), \quad (2)$$

where θ_t is the estimated parameter at the t -th update.

It is obvious that using an ensemble approach with a single model for various updates leads to greater computational efficiency compared to considering multiple models. We demonstrate that this approach not only improves performance but also provides stability, as reported in the experimental section.

We combine the above three techniques—1) mini-batch increment, 2) truncated loss, and 3) loss ensemble at various updates—to propose our method, which we term *Adaptive Loss Truncation with Batch Increment (ALTBI)*. The pseudo algorithm of ALTBI is presented in Algorithm 1.

Choice of DGM framework There are numerous DGMs involved in likelihood maximization, such as VAE-based (Kingma & Welling, 2013; Burda et al., 2016), NF-based (Dinh et al., 2017; Kingma & Dhariwal, 2018), and score-based models (Ho et al., 2020; Song et al., 2021). Among these, we decide to use two approaches: IWAE (Burda et al., 2016) and GLOW (Kingma & Dhariwal, 2018), which are widely used DGMs based on VAE and NF, respectively. Accordingly, their loss functions, $l(\mathbf{x}; \theta)$, would be the ELBO-like upper bound and exact log-likelihood, respectively. Given that one of our method’s key properties is computational efficiency, we do not consider score-based DGMs due to their large model sizes.

4. Theoretical analysis

In this section, we provide theoretical explanations to show that using the mini-batch size increment and truncated loss actually boosts the IM effect. We first state the rigorous definition of the IM effect below.

Assumption 4.1 (IM effect). There exist $0 < a_1 < a_2 < 1$ and $a_3 \in (0, 1 - a_2)$ such that for any parameter θ satisfying $L_i(\theta) \in [a_1, a_2]$, $L_o(\theta) - L_i(\theta) \geq a_3$.

Assumption 4.1 refers to the property that, when a given DGM is trained for a while, there is a gap in risk values between inliers and outliers. A couple of additional yet reasonable assumptions about the gradient are required, which are almost the same as those in Xu et al. (2021).

Assumption 4.2 (Bounded and smooth gradient). Denote the gradients of $l(\theta; \mathbf{x})$ and $L_i(\theta)$ as $\nabla_{\theta} l(\theta; \mathbf{x})$ and

Algorithm 1 ALTBI

In practice, we set

$$(n_0, \gamma, \rho, T_0, T_1, T_2) = (128, 1.03, 0.92, 10, 60, 80).$$

Input: Training data: $\mathcal{D}^{\text{tr}} = \{\mathbf{x}_j\}_{j=1}^n$, parameters of a given DGM: θ , initial mini-batch size: n_0 , mini-batch increment: γ , quantile value: ρ , learning rate: η , three time steps: T_0, T_1 , and T_2 .

- 1: Initialize θ_0 .
- 2: Phase 1: Warm-up
- 3: **for** ($t = 1$ to T_0) **do**
- 4: Draw a mini-batch with the fixed size of n_0 , $\mathcal{D}_t = \{\mathbf{x}_j^{\text{mb}}\}_{j=1}^{n_0}$, from \mathcal{D}^{tr} .
Calculate the loss function:
 $\hat{L}(\theta_0; \mathcal{D}_t) = \frac{1}{n_0} \sum_{j=1}^{n_0} l(\theta_0; \mathbf{x}_j^{\text{mb}})$.
Update θ_0 :
 $\theta_0 \leftarrow \theta_0 - \eta \cdot \nabla_{\theta} \hat{L}(\theta_0; \mathcal{D}_t)$.
- 5: **end for**
- 6: Phase 2: Enhancement of IM effect
- 7: **for** ($t = 1$ to T_2) **do**
- 8: Draw a mini-batch with a size of $n_t = n_0 \gamma^{t-1}$, $\mathcal{D}_t = \{\mathbf{x}_j^{\text{mb}}\}_{j=1}^{n_t}$ from \mathcal{D}^{tr} .
Set the threshold $\tau_t = L_i(\theta_{t-1})$. // In practice, we choose τ_t as $(100 \times \rho)$ -percentile of $\{l(\theta_{t-1}; \mathbf{x}_j)\}_{j=1}^{n_t}$.
Compute truncated loss $\hat{L}(\theta_{t-1}, \tau_t)$ as (1)
Update θ_t :
 $\theta_t \leftarrow \theta_{t-1} - \eta \cdot \nabla_{\theta} \hat{L}(\theta_{t-1}, \tau_t)$.
- 9: **if** ($t > T_1$) **then**
- 10: Incorporate the per-sample loss values to the final ALTBI scores as (2)
- 11: **end if**
- 12: **end for**

Output: ALTBI scores of training data: $\{s^{\text{ALTBI}}(\mathbf{x}_j)\}_{j=1}^n$

$\nabla_{\theta} L_i(\theta)$, respectively. Then the followings conditions are satisfied:

- (i) For any $\mathbf{x} \in \mathcal{X}$ and $\theta \in \Theta$, there exists a constant $G > 0$, such that

$$\|\nabla_{\theta} l(\theta; \mathbf{x})\| \leq G.$$

- (ii) $L_i(\theta)$ is smooth with a L -Lipschitz continuous gradient, i.e., there exists a constant $L > 0$ such that

$$\|\nabla_{\theta} L_i(\theta) - \nabla_{\theta} L_i(\theta')\| \leq L \|\theta - \theta'\|, \quad \forall \theta, \theta' \in \Theta,$$

- (iii) There exists $\mu > 0$ such that for any $\theta \in \Theta$,

$$2\mu(L_i(\theta) - L_i(\theta_*)) = 2\mu L_i(\theta) \leq \|\nabla_{\theta} L_i(\theta)\|^2,$$

where θ_* is the minimizer of $L_i(\theta)$.

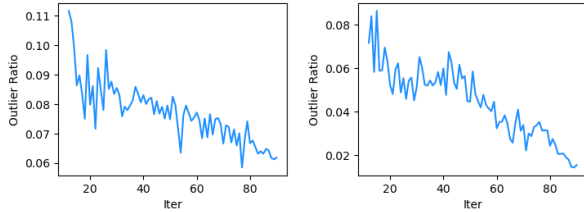


Figure 4. Trace plot of outlier ratio in truncated samples over various iterations. We visualize two datasets: (Left) Cardio and (Right) Shuttle.

The first and second assumptions in Assumption 4.2 refer to the properties that the loss function and inlier risk are smooth. The last assumption is known as the Polyak-Łojasiewicz condition (Polyak, 1964), which is widely considered in the literature related to SGD with deep learning (Yuan et al. (2019) and references therein).

We finally introduce a technical assumption about the loss distribution. We note that this condition is quite weak and can be satisfied in general situations.

Assumption 4.3 (Loss distribution). There is a constant $0 < c < 1$ such that, for any θ , the following inequality holds:

$$\left[E_{P_i} \sqrt{l(\theta; X)} \right]^2 \leq (1 - c)L_i(\theta).$$

Then we have the following proposition, which asserts that if we apply the mini-batch increment and threshold to truncate the loss function, the ratio of outliers included in the truncated loss becomes small. The proof of Proposition 4.1 is provided in the Appendix A.

Proposition 4.1. *At the t -th update, we suppose that the current parameter θ_{t-1} satisfies $a_1 \leq L_i(\theta_{t-1}) \leq a_2\gamma^{-(t-1)}$. For a mini-batch \mathcal{D}_t , we denote the inlier set which is included in the truncated loss as \mathcal{A}_t^r . Similarly, we can define \mathcal{B}_t^r for outliers. Then, under Assumptions 1 to 3 and for a given $\delta > 0$, there exists positive constants c_1 and c_2 not depending on t such that the following two inequalities holds:*

$$|\mathcal{A}_t^r| \geq c_1 n_t \quad \text{and} \quad |\mathcal{B}_t^r| \leq c_2 n_0,$$

with a probability at least $1 - \delta$.

Considering $n_t = n_0\gamma^{t-1}$, Proposition 4.1 indicates that at the t -th update, the ratio of outliers included in the truncated loss cannot exceed $(c_2/c_1) \cdot \gamma^{-(t-1)}$, which decreases toward zero as the update step t increases as long as the IM effect persists at each update. Therefore, our proposed method gradually refines samples in the loss function, leading to the clearer IM effect.

We visualize whether the ratio of outliers actually decreases as the updates proceed. The same learning framework and

hyperparameter settings from Figure 2 are considered, and two datasets are analyzed: Cardio and Shuttle. Figure 4 shows that the outlier ratio in the truncated loss function tends to decrease over updates, providing empirical evidence for Proposition 4.1.

We note that Proposition 4.1 holds provided that the inlier risk is sufficiently small, i.e., smaller than $a_2\gamma^{-(t-1)}$. Next theoretical result deals with the guarantee that the inlier risk indeed decreases over updates with high probability. The proof is provided in Appendix A.

Proposition 4.2. *At the t -th update, we suppose that all the assumptions considered in Proposition 4.1 hold. Then for a given $\delta > 0$, there exists a learning rate $\eta > 0$ such that $L_i(\theta_t) \leq a_2\gamma^{-t}$ with a probability at least $1 - \delta$.*

The above proposition implies that if the previously estimated DGM satisfies the IM effect with a small inlier risk, then the subsequent estimated DGM has a smaller inlier risk with a factor of γ .

Suppose that the IM effect starts to be observed with the estimated parameter after warm-up step, i.e., $a_1 \leq L_i(\theta_0) \leq a_2$. Then, Proposition 4.2 suggests that with a carefully chosen learning rate, ideally, we can observe an enhanced IM effect up to $\lfloor (\log(a_1/a_2))/(\log(1/\gamma)) \rfloor$ consecutive updates.

5. Experiments

We validate the superiority of our proposed method by analyzing an extensive set of 57 datasets, including image, text, and tabular data. We prove that ALTBI is the state-of-the-art solution for various types of data with its high computational efficiency compared to other recent methods. In each experiments, we report the averaged results based on three trials with random parameter initializations. We use the PyTorch framework to run our algorithm using a single NVIDIA TITAN XP GPU.

Dataset description We analyze all 57 outlier detection benchmark datasets from ADBench (Han et al., 2022), including tabular, image, and text data. And as done in Kim et al. (2024), we conduct the min-max scaling to preprocess each dataset. We first consider 46 widely used tabular datasets that cover various application domains, including healthcare, finance, and astronautics. Additionally, we include five benchmark datasets commonly used in the field of natural language processing (NLP): 20news, Agnews, Amazon, IMDB, and Yelp. For these datasets, we utilize embedding features of these datasets via BERT (Devlin et al., 2019) or RoBERTa (Liu et al., 2019), both publicly accessible in ADBench. We finally analyze six image datasets: CIFAR10, MNIST-C, MVTec-AD, SVHN, MNIST, and FMNIST. These datasets are analyzed using the embedding features extracted by the ViT (Dosovitskiy et al., 2021), also

available in ADBench. The detailed information about all the datasets is provided in the Appendix B and Han et al. (2022).

Baseline We mainly compare our method with ODIM (Kim et al., 2024), and also consider other baselines compared in the study. These methods contain traditional machine-learning-based approaches whose implementations are provided in ADBench, including kNN (Ramaswamy et al., 2000), LOF (Breunig et al., 2000b), OCSVM (Schölkopf et al., 2001), CBLOF (He et al., 2003), PCA (Shyu et al., 2003), FeatureBagging (Lazarevic & Kumar, 2005), IForest (Liu et al., 2008), MCD (Fauconnier & Haesbroeck, 2009), HBOS (Goldstein & Dengel, 2012), LODA (Pevný, 2016), COPOD (Li et al., 2020), and ECOD (Li et al., 2022).

And we also consider two deep learning-based UOD methods, DAGMM (Zong et al., 2018) and DeepSVDD (Ruff et al., 2018), both of which can be implemented through ADBench. Additionally, we evaluate our method against more recent deep learning approaches beyond ADBench, such as DROCC (Goyal et al., 2020), ICL (Shenkar & Wolf, 2022), GOAD (Bergman & Hoshen, 2020), DTE (Livernoche et al., 2023), and ODIM (Kim et al., 2024).

Implementation details As mentioned previously, we use two likelihood-based DGM frameworks: 1) IWAE (Burda et al., 2016), an ELBO-based model and 2) GLOW (Nalisnick et al., 2019b), an NF-based model. IWAE uses multiple latent vectors to make the objective function tighter than the standard ELBO. We use the same DNN architecture for IWAE as in Kim et al. (2024), but set the number of the latent samples K to two. Detailed descriptions of the architectures and loss functions are presented in Appendix B. And GLOW (Kingma & Dhariwal, 2018) introduces invertible 1×1 convolution filters to create normalizing flows with high complexity. The architecture considered in Nalisnick et al. (2019b) is used, and we reshape each dataset into a squared form to apply this architecture.

For the optimizer, we use Adam (Kingma & Ba, 2014) with a learning rate of $1e-3$. Throughout our experimental analysis, we fix the hyperparameters, necessary for our proposed method— $(n_0, \gamma, \rho, T_0, T_1, T_2)$ —to $(128, 1.03, 0.92, 10, 60, 80)$, unless stated otherwise. Performance results for other hyperparameter values are provided in the ablation studies.

5.1. Performance results

We evaluate the outlier detection performance of ALTBI with IWAE (ALTBI-I) and GLOW (ALTBI-G) in comparison with other baselines. For each dataset, the mean and standard deviation of outlier detection AUC and PRAUC over three different implementations are measured. We re-

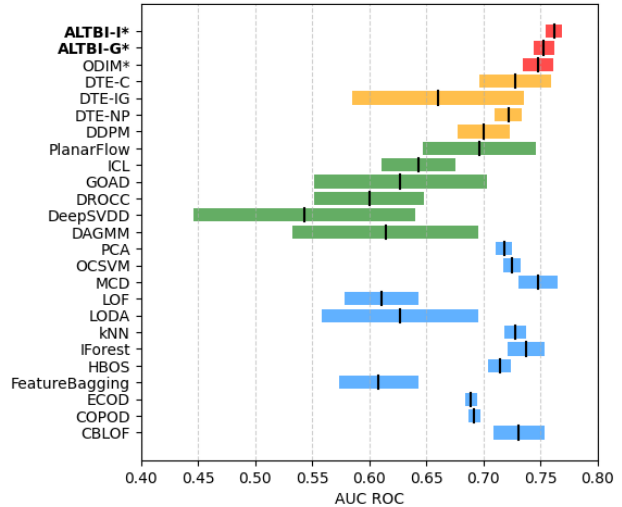


Figure 5. Averaged AUC results, including means and standard deviations, across 57 datasets from ADBench over three different implementations. We mark an asterisk (*) next to methods for our own implementations. Color scheme: red (IM-based), orange (diffusion-based), green (deep-learning-based), blue (machine-learning-based).

port the averaged means and standard deviations of AUC across all datasets in Figure 5. Detailed results for each dataset, including PRAUC, are summarized in Appendix B. We acknowledge that we implemented ALTBI and ODIM ourselves, while all other baseline results are referenced from the Appendix in Livernoche et al. (2023).

Figure 5 shows that the scores of ALTBI-I achieves the best performance, followed by ALTBI-G, both outperforming all other baselines. Considering the computational efficiency of IWAE compared to GLOW, ALTBI-I could be a more favorable method as a UOD solver. Additionally, our method showcases smaller standard deviations compared to other baselines. These results indicate that ALTBI has superior and stable performance across various data types in empirical experiments, again highlighting ALTBI as a off-the-shelf method for UOD.

5.2. Ablation studies

We perform further experiments to explore the impact of hyperparameter choices on ALTBI’s performance across the ADBench datasets and the results are presented in Figure 6. Detailed results can be found in the Appendix B.

- ① The performance improves as the truncation percentage increases up to 8%, but it starts to decline afterward.
- ② Increasing the mini-batch size by a factor of $\gamma = 1.03$ at each update leads to optimal performance.
- ③ Performance is best when $K = 2$ in IWAE, and it tends to decline as K increases further.

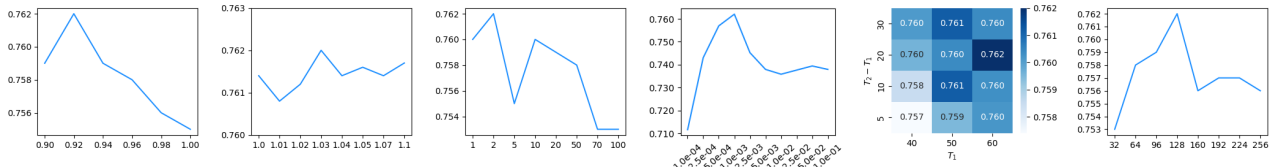


Figure 6. (From left to right) 1) AUC scores with various values of ρ . 2) AUC scores with various values of γ . 3) AUC scores with various values of K in IWAE. 4) AUC scores with various values of learning rate. 5) Heatmap of AUC scores for ensembling with various values of T_1 and $T_1 - T_2$. 6) AUC scores with various values of n_0 .

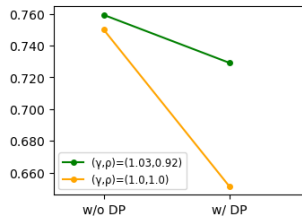


Figure 7. The impact of mini-batch increment and loss truncation when applying an DP-SGD algorithm.

- ④ The learning rate increases up to $1e - 3$, resulting in continuous performance improvement, but after that, performance decreases and stabilizes.
- ⑤ Finding appropriate values of T_1 and T_2 for ensembling within a DGM single model affects ALTBI’s performance but the impact is not significant.
- ⑥ Increasing n_0 enhances ALTBI’s performance up to a value of 128, after which the performance begins to decline and stabilize.
- ⑦ Additionally, we empirically find that ALTBI achieve near state-of-the-art performance in solving SSOD tasks as well. We provide verification of this in Appendix B.

5.3. Further discussions: Robustness of ALTBI in DP

A representative method to ensure that a given algorithm satisfies differential privacy (DP) is by training with the DP-SGD algorithm (Abadi et al., 2016) instead of conventional SGDs. This involves clipping the gradient norm for each per-sample loss and adding Gaussian noise. For a given loss function $\tilde{l}(\theta; \mathbf{x})$, this operation can be formularized as

$$\text{Clip}(\nabla_{\theta} \tilde{l}(\theta; \mathbf{x}); C) + \mathcal{N}(0, \sigma^2 C^2 I),$$

where $C > 0$ is a clipping constant and $\sigma > 0$ controls the noise amount.

We note that ALTBI utilizes $\tilde{l}(\theta; \mathbf{x}) = l(\theta; \mathbf{x})I(l(\theta; \mathbf{x}) \leq \tau)$. When a sample is filtered out from the truncated loss, its gradient is already clipped to have a norm of zero. Since outliers are mostly excluded by the truncated loss, leading to their gradients being clipped to zero, we can infer that incorporating DP-SGD into ALTBI preserves the inliers’

information relative to outliers, making ALTBI inherently robust when implementing DP-SGD.

To validate our claim, we conduct an additional experiment by analyzing 20 tabular datasets. We consider two versions of ALTBI: one that applies mini-batch increment and truncated loss, i.e., $(\gamma, \rho) = (1.03, 0.92)$, and one that does not, i.e., $(\gamma, \rho) = (1.0, 1.0)$. As a measure of DP, we adopt (ϵ, δ) -DP, and with a fixed $\delta = 1e - 5$, we train them using a DP-SGD algorithm until the cumulative privacy budget $\epsilon \leq 10$ holds. Then we compare the averaged outlier detection AUC values in Figure 7. The modified ALTBI for DP and detailed results are provided in Appendix B.

Figure 7 shows that increasing mini-batch sizes and using the truncated loss function yields more robust performance when applying the DP algorithm, indicating that combining ALTBI and DP has a synergistic effect.

6. Concluding remarks

In this study, we developed a novel UOD method called ALTBI, which maximally exploits the IM effect. By introducing two key techniques—gradually increasing the mini-batch size and adopting an adaptive threshold to truncate the loss function—ALTBI demonstrated superior and stable outlier detection performance across various datasets while maintaining computational efficiency. Extensive experiments validated ALTBI’s state-of-the-art results, making it a robust and effective solution for UOD. Several studies have extended outlier detection tasks to scenarios where a few outliers with known outlier information are accessible (Ruff et al., 2020; Kim et al., 2024). Applying our method to the more complex case where some labeled outliers are wrongly annotated would be an interesting direction for future work.

References

- Abadi, M., Chu, A., Goodfellow, I., McMahan, H. B., Mironov, I., Talwar, K., and Zhang, L. Deep learning with differential privacy. In *Proceedings of the 2016 ACM SIGSAC conference on computer and communications security*, pp. 308–318, 2016.

- Bergman, L. and Hoshen, Y. Classification-based anomaly detection for general data. In *International Conference on Learning Representations*, 2020.
- Breunig, M. M., Kriegel, H.-P., Ng, R. T., and Sander, J. Lof: Identifying density-based local outliers. *SIGMOD Rec.*, 29(2):93–104, may 2000a. ISSN 0163-5808. doi: 10.1145/335191.335388.
- Breunig, M. M., Kriegel, H.-P., Ng, R. T., and Sander, J. Lof: identifying density-based local outliers. In *Proceedings of the 2000 ACM SIGMOD international conference on Management of data*, pp. 93–104, 2000b.
- Burda, Y., Grosse, R. B., and Salakhutdinov, R. Importance weighted autoencoders. In *4th International Conference on Learning Representations, ICLR 2016, Conference Track Proceedings*, 2016.
- Chen, T., Kornblith, S., Norouzi, M., and Hinton, G. A simple framework for contrastive learning of visual representations. In *Proceedings of the 37th International Conference on Machine Learning*, volume 119 of *Proceedings of Machine Learning Research*, pp. 1597–1607. PMLR, 13–18 Jul 2020.
- Chung, F. and Lu, L. Concentration inequalities and martingale inequalities: a survey. *Internet mathematics*, 3(1): 79–127, 2006.
- Devlin, J., Chang, M.-W., Lee, K., and Toutanova, K. BERT: Pre-training of deep bidirectional transformers for language understanding. In *Proceedings of the 2019 Conference of the North American Chapter of the Association for Computational Linguistics: Human Language Technologies, Volume 1 (Long and Short Papers)*, pp. 4171–4186. Association for Computational Linguistics, June 2019.
- Dinh, L., Krueger, D., and Bengio, Y. NICE: non-linear independent components estimation. In *3rd International Conference on Learning Representations, ICLR 2015, Workshop Track Proceedings*, 2015.
- Dinh, L., Sohl-Dickstein, J., and Bengio, S. Density estimation using real NVP. In *5th International Conference on Learning Representations, ICLR 2017, Conference Track Proceedings*. OpenReview.net, 2017.
- Dosovitskiy, A., Beyer, L., Kolesnikov, A., Weissenborn, D., Zhai, X., Unterthiner, T., Dehghani, M., Minderer, M., Heigold, G., Gelly, S., Uszkoreit, J., and Houlsby, N. An image is worth 16x16 words: Transformers for image recognition at scale. In *9th International Conference on Learning Representations, ICLR 2021*. OpenReview.net, 2021.
- Dwork, C. Differential privacy. In *Automata, Languages and Programming*, pp. 1–12, Berlin, Heidelberg, 2006. Springer Berlin Heidelberg. ISBN 978-3-540-35908-1.
- Fauconnier, C. and Haesbroeck, G. Outliers detection with the minimum covariance determinant estimator in practice. *Statistical Methodology*, 6(4):363–379, 2009.
- Ghadimi, S., Lan, G., and Zhang, H. Mini-batch stochastic approximation methods for nonconvex stochastic composite optimization. *Mathematical Programming*, 155(1): 267–305, 2016.
- Golan, I. and El-Yaniv, R. Deep anomaly detection using geometric transformations. *arXiv preprint arXiv:1805.10917*, 2018.
- Goldstein, M. and Dengel, A. Histogram-based outlier score (hbos): A fast unsupervised anomaly detection algorithm. *KI-2012: poster and demo track*, 1:59–63, 2012.
- Goyal, S., Raghunathan, A., Jain, M., Simhadri, H. V., and Jain, P. DROCC: deep robust one-class classification. In *Proceedings of the 37th International Conference on Machine Learning, ICML 2020*, volume 119 of *Proceedings of Machine Learning Research*, pp. 3711–3721. PMLR, 2020.
- Han, S., Hu, X., Huang, H., Jiang, M., and Zhao, Y. Ad-bench: Anomaly detection benchmark. In *Neural Information Processing Systems (NeurIPS)*, 2022.
- He, Z., Xu, X., and Deng, S. Discovering cluster-based local outliers. *Pattern recognition letters*, 24(9-10):1641–1650, 2003.
- Ho, J., Jain, A., and Abbeel, P. Denoising diffusion probabilistic models. In *Advances in Neural Information Processing Systems 33: Annual Conference on Neural Information Processing Systems 2020, NeurIPS 2020*, 2020.
- Kim, D., Hwang, J., and Kim, Y. On casting importance weighted autoencoder to an em algorithm to learn deep generative models. In *International Conference on Artificial Intelligence and Statistics*, pp. 2153–2163. PMLR, 2020.
- Kim, D., Hwang, J., Lee, J., Kim, K., and Kim, Y. Odin: Outlier detection via likelihood of under-fitted generative models, 2024. URL <https://arxiv.org/abs/2301.04257>.
- Kingma, D. P. and Ba, J. Adam: A method for stochastic optimization. *arXiv preprint arXiv:1412.6980*, 2014.
- Kingma, D. P. and Dhariwal, P. Glow: Generative flow with invertible 1x1 convolutions. In Bengio, S., Wallach, H. M., Larochelle, H., Grauman, K., Cesa-Bianchi, N., and Garnett, R. (eds.), *Advances in Neural Information Processing Systems 31: Annual Conference on Neural Information Processing Systems 2018, NeurIPS 2018*, pp. 10236–10245, 2018.

- Kingma, D. P. and Welling, M. Auto-encoding variational bayes. *arXiv preprint arXiv:1312.6114*, 2013.
- Lan, C. L. and Dinh, L. Perfect density models cannot guarantee anomaly detection. *Entropy*, 23(12):1690, 2021. doi: 10.3390/E23121690.
- Lazarevic, A. and Kumar, V. Feature bagging for outlier detection. In *Proceedings of the eleventh ACM SIGKDD international conference on Knowledge discovery in data mining*, pp. 157–166, 2005.
- Li, Z., Zhao, Y., Botta, N., Ionescu, C., and Hu, X. Copod: copula-based outlier detection. In *2020 IEEE international conference on data mining (ICDM)*, pp. 1118–1123. IEEE, 2020.
- Li, Z., Zhao, Y., Hu, X., Botta, N., Ionescu, C., and Chen, G. Ecod: Unsupervised outlier detection using empirical cumulative distribution functions. *IEEE Transactions on Knowledge and Data Engineering*, 2022.
- Liu, F. T., Ting, K. M., and Zhou, Z.-H. Isolation forest. In *2008 eighth IEEE international conference on data mining*, pp. 413–422. IEEE, 2008.
- Liu, Y., Ott, M., Goyal, N., Du, J., Joshi, M., Chen, D., Levy, O., Lewis, M., Zettlemoyer, L., and Stoyanov, V. Roberta: A robustly optimized BERT pretraining approach. *CoRR*, abs/1907.11692, 2019.
- Livernoche, V., Jain, V., Hezaveh, Y., and Ravanbakhsh, S. On diffusion modeling for anomaly detection. *CoRR*, abs/2305.18593, 2023. doi: 10.48550/ARXIV.2305.18593.
- Nalisnick, E., Matsukawa, A., Teh, Y. W., and Lakshminarayanan, B. Detecting out-of-distribution inputs to deep generative models using typicality, 2019a.
- Nalisnick, E. T., Matsukawa, A., Teh, Y. W., Görür, D., and Lakshminarayanan, B. Do deep generative models know what they don’t know? In *7th International Conference on Learning Representations, ICLR 2019*. OpenReview.net, 2019b.
- Pevný, T. Loda: Lightweight on-line detector of anomalies. *Machine Learning*, 102:275–304, 2016.
- Polyak, B. T. Gradient methods for solving equations and inequalities. *USSR Computational Mathematics and Mathematical Physics*, 4(6):17–32, 1964.
- Ramaswamy, S., Rastogi, R., and Shim, K. Efficient algorithms for mining outliers from large data sets. In *Proceedings of the 2000 ACM SIGMOD international conference on Management of data*, pp. 427–438, 2000.
- Ruff, L., Vandermeulen, R., Goernitz, N., Deecke, L., Siddiqui, S. A., Binder, A., Müller, E., and Kloft, M. Deep one-class classification. In *Proceedings of the 35th International Conference on Machine Learning*, volume 80 of *Proceedings of Machine Learning Research*, pp. 4393–4402. PMLR, 10–15 Jul 2018.
- Ruff, L., Vandermeulen, R. A., Görnitz, N., Binder, A., Müller, E., Müller, K.-R., and Kloft, M. Deep semi-supervised anomaly detection. In *International Conference on Learning Representations*, 2020.
- Schölkopf, B., Platt, J., Shawe-Taylor, J., Smola, A., and Williamson, R. Estimating support of a high-dimensional distribution. *Neural Computation*, 13:1443–1471, 07 2001. doi: 10.1162/089976601750264965.
- Shenkar, T. and Wolf, L. Anomaly detection for tabular data with internal contrastive learning. In *International conference on learning representations*, 2022.
- Shyu, M.-L., Chen, S.-C., Sarinnapakorn, K., and Chang, L. A novel anomaly detection scheme based on principal component classifier. In *Proceedings of the IEEE foundations and new directions of data mining workshop*, pp. 172–179. IEEE Press, 2003.
- Song, Y., Sohl-Dickstein, J., Kingma, D. P., Kumar, A., Ermon, S., and Poole, B. Score-based generative modeling through stochastic differential equations. In *9th International Conference on Learning Representations, ICLR 2021*. OpenReview.net, 2021. URL <https://openreview.net/forum?id=PXTIG12RRHS>.
- Tack, J., Mo, S., Jeong, J., and Shin, J. Csi: Novelty detection via contrastive learning on distributionally shifted instances. In *Advances in Neural Information Processing Systems*, volume 33, pp. 11839–11852. Curran Associates, Inc., 2020.
- Tax, D. M. and Duin, R. P. Support vector data description. *Machine learning*, 54:45–66, 2004.
- Xu, Y., Shang, L., Ye, J., Qian, Q., Li, Y., Sun, B., Li, H., and Jin, R. Dash: Semi-supervised learning with dynamic thresholding. In *Proceedings of the 38th International Conference on Machine Learning, ICML 2021*, volume 139 of *Proceedings of Machine Learning Research*, pp. 11525–11536. PMLR, 2021. URL <http://proceedings.mlr.press/v139/xu21e.html>.
- Yousefpour, A., Shilov, I., Sablayrolles, A., Testuggine, D., Prasad, K., Malek, M., Nguyen, J., Ghosh, S., Bharadwaj, A., Zhao, J., Cormode, G., and Mironov, I. Opacus: User-friendly differential privacy library in PyTorch. *arXiv preprint arXiv:2109.12298*, 2021.

- Yuan, Z., Yan, Y., Jin, R., and Yang, T. Stagewise training accelerates convergence of testing error over SGD. In *Advances in Neural Information Processing Systems 32: Annual Conference on Neural Information Processing Systems 2019, NeurIPS 2019*, pp. 2604–2614, 2019. URL <https://proceedings.neurips.cc/paper/2019/hash/fcdf25d6e191893e705819b177cddea0-Abstract.html>.
- Zhai, S., Cheng, Y., Lu, W., and Zhang, Z. Deep structured energy based models for anomaly detection. In *International conference on machine learning*, pp. 1100–1109. PMLR, 2016.
- Zhou, C. and Paffenroth, R. C. Anomaly detection with robust deep autoencoders. In *Proceedings of the 23rd ACM SIGKDD International Conference on Knowledge Discovery and Data Mining, Halifax, NS*, pp. 665–674. ACM, 2017. doi: 10.1145/3097983.3098052. URL <https://doi.org/10.1145/3097983.3098052>.
- Zong, B., Song, Q., Min, M. R., Cheng, W., Lumezanu, C., Cho, D., and Chen, H. Deep autoencoding gaussian mixture model for unsupervised anomaly detection. In *International Conference on Learning Representations*, 2018.

A. Proof of Theoretical results

Our theoretical results and their proofs are similar to Theorem 1 in Xu et al. (2021). Before starting to prove Proposition 1&2, we first state three lemmas that are used throughout our proofs.

Lemma A.1. *If the IM assumption is satisfied, there exists $a_4 > 0$ such that the following inequality holds:*

$$P_o(l(\theta; X) \leq L_i(\theta)) \leq a_4 \cdot L_i(\theta). \quad (3)$$

proof) We have the following inequalities:

$$\begin{aligned} P_o(l(\theta; X) \leq L_i(\theta)) &= P_o(l(\theta; X) - L_o(\theta) \leq -(L_o(\theta) - L_i(\theta))) \\ &\leq P_o(|l(\theta; X) - L_o(\theta)| \geq (L_o(\theta) - L_i(\theta))) \\ &\stackrel{\text{(Markov's Ineq.)}}{\leq} \frac{\mathbb{E}_o |l(\theta; X) - L_o(\theta)|}{L_o(\theta) - L_i(\theta)} \\ &\leq \frac{\mathbb{E}_o |l(\theta; X)| + L_o(\theta)}{L_o(\theta) - L_i(\theta)} \leq \frac{2L_o(\theta)}{a_3}. \end{aligned}$$

Since $a_1 \leq L_i(\theta)$, we have $L_o(\theta) \leq 1 \leq L_i(\theta)/a_1$. Therefore, we have

$$P_o(l(\theta; X) \leq L_i(\theta)) \leq \frac{2L_o(\theta)}{a_3} \leq \frac{2}{a_1 a_3} L_i(\theta),$$

and the proof is completed with $a_4 = 2/(a_1 a_3)$. \square

Lemma A.2 (Conditional version of Theorem 3.6 in Chung & Lu (2006)). *Suppose that Y_i for $i \in [n]$ are random variables satisfying $Y_i \leq M$ and \mathcal{H} is a given σ -algebra. Let assume that the conditional expectations $\mathbb{E}(Y_i|\mathcal{H})$ s are independent. Let $Y = \sum_{i=1}^n Y_i$ and $\|Y\|_{\mathcal{H}} = \sqrt{\sum_{i=1}^n \mathbb{E}(Y_i^2|\mathcal{H})}$. Then, for any $\lambda > 0$, we have*

$$P\left(Y \geq \mathbb{E}(Y|\mathcal{H}) + \lambda \mid \mathcal{H}\right) \leq \exp\left(-\frac{\lambda^2}{2(\|Y\|_{\mathcal{H}}^2 + M\lambda/3)}\right) \text{ a.s..}$$

Lemma A.3 (Conditional version of Lemma 4 in Ghadimi et al. (2016)). *Suppose that Y_i s, $i \in [n]$, are random variables with mean zero and \mathcal{H} is a given σ -algebra. Let us assume that there exist positive values $\sigma_i^2 > 0$, $i \in [n]$, such that $\mathbb{E}(Y_i^2) \leq \sigma_i^2$. We also assume that the conditional expectations $\mathbb{E}(Y_i|\mathcal{H})$ s are independent. Then for any $\lambda > 0$, the following holds:*

$$P\left(\left\|\sum_{i=1}^n Y_i\right\| \geq \lambda \sum_{i=1}^n \sigma_i^2 \mid \mathcal{H}\right) \leq \frac{1}{\lambda} \text{ a.s..}$$

A.1. Proof of Proposition 4.1

※We prove this proposition with a probability of $1 - 4\delta$. Transforming $1 - 4\delta$ to $1 - \delta$ is trivial by substituting δ with $\delta/4$.

Before we carry out our analysis, we define a few important constants

$$\begin{aligned} C_1 &= \sqrt{\frac{\log(2/\delta)}{2c^2(1-\alpha)n_0}}, \\ C_2 &= \max\left(\sqrt{\frac{\log(2/\delta)}{2(1-\alpha)^2n_0}}, \sqrt{\frac{\log(2/\delta)}{2\alpha^2n_0}}\right), \\ C_3 &= c(1-\alpha)(1-C_1)(1-C_2), \\ C_4 &= \left(4\alpha(1+C_2)a_2a_4 + \frac{1}{3}\log(1/\delta)\right), \end{aligned}$$

where a_4 is the same constant as in Lemma A.1. For the mini-batch $\mathcal{D}_t = \{X_1, \dots, X_{n_t}\}$ with $n_t = n_0 \gamma^{t-1}$ training examples sampled from \mathcal{D} , we divide it into two sets for the analysis use only, i.e. set \mathcal{A}_t that includes examples sampled from \mathcal{P}_i and set \mathcal{B}_t that includes examples sampled from \mathcal{P}_o . We furthermore denote by \mathcal{A}_t^τ and \mathcal{B}_t^τ the subset of examples in \mathcal{A}_t and \mathcal{B}_t whose loss is smaller than the given threshold τ_t , i.e.

$$\mathcal{A}_t^\tau = \{X \in \mathcal{A}_t : l(\theta_{t-1}; X) \leq \tau_t\},$$

$$\mathcal{B}_t^\tau = \{X \in \mathcal{B}_t : l(\theta_{t-1}; X) \leq \tau_t\},$$

where $\tau_t = L_i(\theta_{t-1})$ and θ_{t-1} is the currently estimated parameter at the $(t-1)$ -th update. We assume that $L_i(\theta_{t-1}) \leq a_2 \gamma^{-(t-1)}$. Evidently, the samples used for computing \mathbf{g}_t are the union of \mathcal{A}_t^τ and \mathcal{B}_t^τ . The following result bounds the size of \mathcal{A}_t^τ and \mathcal{B}_t^τ . With a probability $1 - 4\delta$. We have

$$|\mathcal{A}_t^\tau| \geq C_3 n_t = C_3 n_0 \gamma^{t-1}, \quad |\mathcal{B}_t^\tau| \leq C_4 n_0,$$

where C_3 and C_4 are defined above.

(i) Lower bound of \mathcal{A}_t^τ By Hoeffding's inequality, for any $t > 0$, we have

$$P_*(|\mathcal{A}_t| - (1 - \alpha)n_t \geq -t) \geq P_*(|\mathcal{A}_t| - (1 - \alpha)n_t \leq t) \geq 1 - 2\exp(-2t^2/n_t).$$

By substituting $t = \sqrt{\frac{n_t \log(2/\delta)}{2}}$ with $\delta > 0$, we have

$$|\mathcal{A}_t| \geq (1 - \alpha)n_t \left(1 - \sqrt{\frac{\log(2/\delta)}{2(1 - \alpha)^2 n_t}}\right) \geq (1 - \alpha)(1 - C_2)n_t, \quad (4)$$

with a probability at least $1 - \delta$.

By using the general Markov inequality,

$$P_i(l(\theta_{t-1}; X) \leq \tau_t) = 1 - P_i(l(\theta_{t-1}; X) \geq \tau_t) \geq 1 - \frac{\mathbb{E}_{P_i}[\sqrt{l(\theta_{t-1}; X)}]}{\sqrt{L_i(\theta_{t-1})}} \geq c,$$

where the last inequality holds due to Jensen's inequality. Let $\mathcal{F}_t := \mathcal{F}(I(X_j \in \mathcal{X}_i), j \in [n_t])$. We apply the conditional Hoeffding's inequality to achieve the following: for any $t > 0$,

$$\begin{aligned} P_*\left(|\mathcal{A}_t^\tau| - c|\mathcal{A}_t| \geq -t \mid \mathcal{F}_t\right) &\geq P\left(\left||\mathcal{A}_t^\tau| - \mathbb{E}(|\mathcal{A}_t^\tau|)\right| \leq t \mid \mathcal{F}_t\right) \\ &\geq 1 - 2\exp\left(-\frac{2t^2}{|\mathcal{A}_t|}\right) \text{ a.s.} \end{aligned}$$

With $t = \sqrt{\frac{|\mathcal{A}_t|}{2} \log(2/\delta)}$,

$$P_*\left(|\mathcal{A}_t^\tau| \geq c|\mathcal{A}_t| \left(1 - \sqrt{\frac{\log(2/\delta)}{2c^2|\mathcal{A}_t|}}\right) \mid \mathcal{F}_t\right) \geq 1 - \delta \text{ a.s.},$$

and hence

$$P_*\left(|\mathcal{A}_t^\tau| \geq c|\mathcal{A}_t| \left(1 - \sqrt{\frac{\log(2/\delta)}{2c^2|\mathcal{A}_t|}}\right)\right) \geq 1 - \delta. \quad (5)$$

Combining (4) and (5), we have

$$\begin{aligned} |\mathcal{A}_t^\tau| &\geq c|\mathcal{A}_t| \left(1 - \sqrt{\frac{\log(2/\delta)}{2c^2|\mathcal{A}_t|}}\right) \\ &\geq c(1 - \alpha)(1 - C_2)n_t \left(1 - \sqrt{\frac{\log(2/\delta)}{2c^2(1 - \alpha)(1 - C_2)n_t}}\right) \\ &\geq c(1 - \alpha)(1 - C_2)(1 - C_1)n_t \\ &= C_3 n_t, \end{aligned} \quad (6)$$

with a probability at least $1 - 2\delta$.

(ii) **Upper bound of \mathcal{B}_t^τ** And by Hoeffding's inequality, we also have

$$P_*(|\mathcal{B}_t| - \alpha n_t \leq t) \geq P_*(||\mathcal{B}_t| - \alpha n_t| \geq t) \geq 1 - 2 \exp(-2t^2/n_t).$$

By substituting $t = \sqrt{\frac{n_t \log(2/\delta)}{2}}$, we have

$$|\mathcal{B}_t| \leq \alpha n_t \left(1 + \sqrt{\frac{\log(2/\delta)}{2\alpha^2 n_t}} \right) \leq \alpha(1 + C_2)n_t, \quad (7)$$

with a probability at least $1 - \delta$. Also, by using Lemma A.1, the following inequalities hold:

$$P_o(l(\theta_{t-1}; X) \leq \tau_t) = P_o(l(\theta_{t-1}; X) \leq L_i(\theta_{t-1})) \stackrel{(Lem.A.1)}{\leq} a_4 \cdot L_i(\theta_{t-1}) \leq a_2 a_4 \gamma^{-(t-1)}. \quad (8)$$

Let $\mathcal{G}_t := \mathcal{F}(I(X_j \in \mathcal{X}_o), j \in [n_t])$. We can bound the expectation of $|\mathcal{B}_t^\tau|$ given \mathcal{G}_t , i.e.,

$$\begin{aligned} \mathbb{E}_* \left[|\mathcal{B}_t^\tau| \middle| \mathcal{G}_t \right] &= \mathbb{E}_* \left[\sum_{X \in \mathcal{B}_t} I(l(\theta_{t-1}; X) \leq \tau_t) \middle| \mathcal{G}_t \right] \\ &\leq |\mathcal{B}_t| P_o(l(\theta_{t-1}; X) \leq \tau_t) \stackrel{(8)}{\leq} |\mathcal{B}_t| a_2 a_4 \gamma^{-(t-1)} \text{ a.s.} \end{aligned} \quad (9)$$

Also, by using Lemma A.2, for any $\lambda > 0$, the following inequality holds:

$$P_* \left(|\mathcal{B}_t^\tau| \leq \mathbb{E}_* [|\mathcal{B}_t^\tau| \middle| \mathcal{G}_t] + \lambda \middle| \mathcal{G}_t \right) \geq 1 - \exp \left(-\frac{\lambda^2}{2\mathbb{E}_* [|\mathcal{B}_t^\tau| \middle| \mathcal{G}_t] + \lambda/3} \right) \text{ a.s.}$$

For a given $\delta > 0$, by substituting $\lambda = \frac{1}{3} \log(1/\delta) + \sqrt{\frac{1}{9} \log^2(1/\delta) + 2 \log(1/\delta) \mathbb{E}_* [|\mathcal{B}_t^\tau| \middle| \mathcal{G}_t]}$, we have

$$P_* \left(|\mathcal{B}_t^\tau| \leq \mathbb{E}_* [|\mathcal{B}_t^\tau| \middle| \mathcal{G}_t] + \frac{1}{3} \log(1/\delta) + \sqrt{\frac{1}{9} \log^2(1/\delta) + 2 \log(1/\delta) \mathbb{E}_* [|\mathcal{B}_t^\tau| \middle| \mathcal{G}_t]} \middle| \mathcal{G}_t \right) \geq 1 - \delta \text{ a.s.,}$$

and hence

$$P_* \left(|\mathcal{B}_t^\tau| \leq \mathbb{E}_* [|\mathcal{B}_t^\tau| \middle| \mathcal{G}_t] + \frac{1}{3} \log(1/\delta) + \sqrt{\frac{1}{9} \log^2(1/\delta) + 2 \log(1/\delta) \mathbb{E}_* [|\mathcal{B}_t^\tau| \middle| \mathcal{G}_t]} \right) \geq 1 - \delta. \quad (10)$$

We combine (7), (9), and (10) to achieve the inequality below:

$$\begin{aligned} |\mathcal{B}_t^\tau| &\leq \mathbb{E}_* [|\mathcal{B}_t^\tau| \middle| \mathcal{G}_t] + \frac{1}{3} \log(1/\delta) + \sqrt{\frac{1}{9} \log^2(1/\delta) + 2 \log(1/\delta) \mathbb{E}_* [|\mathcal{B}_t^\tau| \middle| \mathcal{G}_t]} \\ &\leq 4\mathbb{E}_* [|\mathcal{B}_t^\tau| \middle| \mathcal{G}_t] + \frac{2}{3} \log(1/\delta) \\ &\leq 4|\mathcal{B}_t| a_2 a_4 \gamma^{-(t-1)} + \frac{2}{3} \log(1/\delta) \\ &\leq 4\alpha(1 + C_2)n_0 \gamma^{t-1} a_2 a_4 \gamma^{-(t-1)} + \frac{2}{3} \log(1/\delta) \\ &= 4\alpha(1 + C_2)n_0 a_2 a_4 + \frac{2}{3} \log(1/\delta) \\ &\leq \left(4\alpha(1 + C_2)a_2 a_4 + \frac{1}{3} \log(1/\delta) \right) n_0 = C_4 n_0. \end{aligned} \quad (11)$$

with a probability at least $1 - 2\delta$.

Therefore, with (6) and (11), the proof is completed with $c_1 = C_3$ and $c_2 = C_4$. \square

A.2. Proof of Proposition 4.2

※Similar to the proof of Proposition 1, we prove Proposition 2 with a probability of $1 - 5\delta$. Transforming $1 - 5\delta$ to $1 - \delta$ can be done by using $\delta/5$ instead of δ .

We will demonstrate that, with high probability, $L(\theta_t) \leq a_2\gamma^{-t}$. Let $\mathbf{g}_t = \nabla_{\theta} \widehat{L}(\theta_{t-1}, \tau_t)$. To this end, using the notation of \mathcal{A}_t^r and \mathcal{B}_t^r , we can rewrite \mathbf{g}_t as

$$\mathbf{g}_t = (1 - b_t)\mathbf{g}_t^a + b_t\mathbf{g}_t^b,$$

where $\mathbf{g}_t^a = \frac{1}{|\mathcal{A}_t^r|} \sum_{X \in \mathcal{A}_t^r} \nabla l(\theta_{t-1}; X)$, $\mathbf{g}_t^b = \frac{1}{|\mathcal{B}_t^r|} \sum_{X \in \mathcal{B}_t^r} \nabla l(\theta_{t-1}; X)$, and b_t is the proportion of samples from \mathcal{B}_t^r that

$$b_t = \frac{|\mathcal{B}_t^r|}{|\mathcal{A}_t^r| + |\mathcal{B}_t^r|} \leq \frac{|\mathcal{B}_t^r|}{|\mathcal{A}_t^r|} \leq \frac{c_2}{1 + c_1\gamma^{t-1}} < \frac{c_2}{c_1}\gamma^{-(t-1)},$$

with a probability of at least $1 - 4\delta$ by Proposition 1. Following the classical analysis of non-convex optimization, since $L(\theta)$ is L -smooth by Assumption 2 (ii), we have

$$\begin{aligned} L_i(\theta_t) - L_i(\theta_{t-1}) &\stackrel{(a)}{\leq} \langle \nabla L_i(\theta_{t-1}), \theta_t - \theta_{t-1} \rangle + \frac{L}{2} \|\theta_t - \theta_{t-1}\|^2 \\ &\stackrel{(b)}{=} \frac{\eta}{2} \|\nabla L_i(\theta_{t-1}) - \mathbf{g}_t\|^2 - \frac{\eta}{2} (\|\nabla L_i(\theta_{t-1})\|^2 + (1 - \eta L)\|\mathbf{g}_t\|^2) \\ &\stackrel{(c)}{\leq} \frac{\eta}{2} ((1 - b_t)\|\nabla L_i(\theta_{t-1}) - \mathbf{g}_t^a\|^2 + b_t\|\nabla L_i(\theta_{t-1}) - \mathbf{g}_t^b\|^2) - \frac{\eta}{2} (\|\nabla L_i(\theta_{t-1})\|^2 + (1 - \eta L)\|\mathbf{g}_t\|^2) \\ &\stackrel{(d)}{\leq} \frac{\eta}{2} ((1 - b_t)\|\nabla L_i(\theta_{t-1}) - \mathbf{g}_t^a\|^2 + 4b_tG^2) - \eta\mu L_i(\theta_{t-1}), \end{aligned} \quad (12)$$

where (a) is due to Assumption 2-(i); (b) follows the update of $\theta_t = \theta_{t-1} - \eta\mathbf{g}_t$; (c) is due to the definition of \mathbf{g}_t and the convexity of $\|\cdot\|^2$; (d) follows the Assumption 2-(i),(ii), and $\eta L \leq 1$.

Let $\mathcal{F}_t^r := \mathcal{F}(I(X_j \in \mathcal{A}_t^r), j \in [n_t])$. Then we have

$$\begin{aligned} \mathbb{E}_* \left(\|\mathbf{g}_t^a - \nabla L_i(\theta_{t-1})\|^2 \middle| \mathcal{F}_t^r \right) &= \frac{1}{|\mathcal{A}_t^r|^2} \mathbb{E}_* \left(\left\| \sum_{X \in \mathcal{A}_t^r} (\nabla l(\theta_t; X) - \nabla L(\theta_t)) \right\|^2 \middle| \mathcal{F}_t^r \right) \\ &= \frac{1}{|\mathcal{A}_t^r|^2} \mathbb{E}_* \left(\sum_{X \in \mathcal{A}_t^r} \|\nabla l(\theta_t; X) - \nabla L(\theta_t)\|^2 \middle| \mathcal{F}_t^r \right) \\ &\leq \frac{4G^2}{|\mathcal{A}_t^r|}, \end{aligned}$$

where the last inequality holds due to Assumption 2-(i). For a given $\delta > 0$, by using Lemma A.3 with $\lambda = 1/\delta$, we have

$$P_* \left(P_* \left(\|\mathbf{g}_t^a - \nabla L_i(\theta_{t-1})\|^2 \leq \frac{4G^2}{\delta|\mathcal{A}_t^r|} \middle| \mathcal{F}_t^r \right) \geq 1 - \delta \right) = 1,$$

and hence

$$P_* \left(\|\mathbf{g}_t^a - \nabla L_i(\theta_{t-1})\|^2 \leq \frac{4G^2}{\delta|\mathcal{A}_t^r|} \right) \geq 1 - \delta. \quad (13)$$

We combine (6) and (13) to achieve

$$\|\mathbf{g}_t^a - \nabla L_i(\theta_{t-1})\|^2 \leq \frac{4G^2}{\delta c_1 n_0} \gamma^{-(t-1)}, \quad (14)$$

with a probability of at least $1 - 5\delta$.

Using the above bound in (14), we can further expand the bound in (12) as follows:

$$\begin{aligned} L_i(\theta_t) - L_i(\theta_{t-1}) &\leq \frac{\eta}{2} \left((1 - b_t) \frac{4G^2}{\delta c_1 n_0} \gamma^{-(t-1)} + 4b_t G^2 \right) - \eta \mu L_i(\theta_{t-1}) \\ &\leq \frac{\eta}{2} \left(\frac{4G^2}{\delta c_1 n_0} \gamma^{-(t-1)} + 4G^2 \frac{c_2}{c_1} \gamma^{-(t-1)} \right) - \eta \mu L_i(\theta_{t-1}) \\ &= \frac{2\eta G^2}{c_1} \left(\frac{1}{\delta n_0} + c_2 \right) \gamma^{-(t-1)} - \eta \mu L_i(\theta_{t-1}). \end{aligned}$$

Hence, we have

$$\begin{aligned} L_i(\theta_t) &\leq (1 - \eta \mu) L_i(\theta_{t-1}) + \frac{2\eta G^2}{c_1} \left(\frac{1}{\delta n_0} + c_2 \right) \gamma^{-(t-1)} \\ &\leq \gamma \left[(1 - \eta \mu) a_2 + \frac{2\eta G^2}{c_1} \left(\frac{1}{\delta n_0} + c_2 \right) \right] \gamma^{-t}, \end{aligned}$$

with a probability of at least $1 - 5\delta$. Let us select the learning rate η between the interval given as:

$$\frac{1}{\mu} \left(1 - \frac{1}{2\gamma} \right) \leq \eta \leq \frac{a_2 c_1}{4\gamma G^2 \left(\frac{1}{\delta n_0} + c_2 \right)}.$$

Then, we have

$$\begin{aligned} L_i(\theta_t) &\leq \gamma \left[(1 - \eta \mu) a_2 + \frac{2\eta G^2}{c_1} \left(\frac{1}{\delta n_0} + c_2 \right) \right] \gamma^{-t} \\ &\leq \gamma \left(\frac{a_2}{2\gamma} + \frac{a_2}{2\gamma} \right) \gamma^{-t} \\ &= a_2 \gamma^{-t}, \end{aligned}$$

and the proof is completed. \square

B. Detailed experiment results

B.1. Description of Importance weighted autoencoders (IWAE)

Importance Weighted Autoencoders (IWAE) (Burda et al., 2016) is a variational inference method designed to produce arbitrarily tight lower bounds. For a given input \mathbf{x} , IWAE minimizes the following expression, which leverages multiple samples from the variational distribution $q(\mathbf{z}|\mathbf{x}; \phi)$:

$$-\mathbb{E}_{\mathbf{z}_1, \dots, \mathbf{z}_K \sim q(\mathbf{z}|\mathbf{x}; \phi)} \left[\log \left(\frac{1}{K} \sum_{k=1}^K \frac{p(\mathbf{x}, \mathbf{z}_k; \theta)}{q(\mathbf{z}_k|\mathbf{x}; \phi)} \right) \right],$$

where K is the number of samples. In practice, IWAE approximates this lower bound using the Monte Carlo method, which is expressed as:

$$\hat{L}^{\text{IWAE}}(\theta, \phi; \mathbf{x}) := -\log \left(\frac{1}{K} \sum_{k=1}^K \frac{p(\mathbf{x}, \mathbf{z}_k; \theta)}{q(\mathbf{z}_k|\mathbf{x}; \phi)} \right),$$

where $\mathbf{z}_k \sim q(\mathbf{z}|\mathbf{x}; \phi)$ for $k = 1, \dots, K$. As for the encoder and decoder, as done in Kim et al. (2024), we use two hidden layered DNN architectures with 50 to 100 hidden nodes for each hidden layer. And we set K , the number of samples drawn from the encoder used for constructing the IWAE objective function, to two. We minimize the above loss function with respect to (θ, ϕ) using an SGD-based optimizer such as Adam (Kingma & Ba, 2014).

B.2. Data description

We evaluate a total of 46 tabular datasets, 6 image datasets, and 5 text datasets. These datasets are all obtained from a source known as ADBench. (Han et al., 2022b). Table B.1 provides a summary of the basic information for all datasets we analyze.

Number	Dataset Name	#Samples	#Features	#Anomaly	%Anomaly	Category
1	ALOI	49534	27	1508	3.04	Image
2	annthyroid	7200	6	534	7.42	Healthcare
3	backdoor	95329	196	2329	2.44	Network
4	breastw	683	9	239	34.99	Healthcare
5	campaign	41188	62	4640	11.27	Finance
6	cardio	1831	21	176	9.61	Healthcare
7	Cardiotocography	2114	21	466	22.04	Healthcare
8	celeba	202599	39	4547	2.24	Image
9	census	299285	500	18568	6.2	Sociology
10	cover	286048	10	2747	0.96	Botany
11	donors	619326	10	36710	5.93	Sociology
12	fault	1941	27	673	34.67	Physical
13	fraud	284807	29	492	0.17	Finance
14	glass	214	7	9	4.21	Forensic
15	Hepatitis	80	19	13	16.25	Healthcare
16	http	567498	3	2211	0.39	Web
17	InternetAds	1966	1555	368	18.72	Image
18	Ionosphere	351	32	126	35.9	Oryctognosy
19	landsat	6435	36	1333	20.71	Astronautics
20	letter	1600	32	100	6.25	Image
21	Lymphography	148	18	6	4.05	Healthcare
22	magic.gamma	19020	10	6688	35.16	Physical
23	mammography	11183	6	260	2.32	Healthcare
24	mnist	7603	100	700	9.21	Image
25	musk	3062	166	97	3.17	Chemistry
26	optdigits	5216	64	150	2.88	Image
27	PageBlocks	5393	10	510	9.46	Document
28	pendigits	6870	16	156	2.27	Image
29	Pima	768	8	268	34.9	Healthcare
30	satellite	6435	36	2036	31.64	Astronautics
31	satimage-2	5803	36	71	1.22	Astronautics
32	shuttle	49097	9	3511	7.15	Astronautics
33	skin	245057	3	50859	20.75	Image
34	smtp	95156	3	30	0.03	Web
35	SpamBase	4207	57	1679	39.91	Document
36	speech	3686	400	61	1.65	Linguistics
37	Stamps	340	9	31	9.12	Document
38	thyroid	3772	6	93	2.47	Healthcare
39	vertebral	240	6	30	12.5	Biology
40	vowels	1456	12	50	3.43	Linguistics
41	Waveform	3443	21	100	2.9	Physics
42	WBC	223	9	10	4.48	Healthcare
43	WDBC	367	30	10	2.72	Healthcare
44	Wilt	4819	5	257	5.33	Botany
45	wine	129	13	10	7.75	Chemistry
46	WPBC	198	33	47	23.74	Healthcare
47	yeast	1484	8	507	34.16	Biology
48	CIFAR10	5263	512	263	5	Image
49	FashionMNIST	6315	512	315	5	Image
50	MNIST-C	10000	512	500	5	Image
51	MVTec-AD	5354	512	1258	23.5	Image
52	SVHN	5208	512	260	5	Image
53	Agnews	10000	768	500	5	NLP
54	Amazon	10000	768	500	5	NLP
55	Imdb	10000	768	500	5	NLP
56	Yelp	10000	768	500	5	NLP
57	20news	11905	768	591	4.96	NLP

Table B.1. Description of ADBench datasets

B.3. Detailed AUC and PRAUC results over ADBench datasets

Table B.2- B.5 provide detailed results of averaged AUC and PRAUC for each method over the ADBench datasets in unsupervised and semi-supervised settings.

	CBLOF	COPOD	ECOD	FeatureBagging	HBOS	iForest	kNN	LODA	LOF	MCD	OC5VM	PCA	DAGMM	DeepSVDD	DROCC	GOAD	ICL	PlanarFlow	DDPM	DTE-NP	DTE-IG	DTE-C	ODIM	ALTBI-G	ALTBI-I
aloi	0.556	0.515	0.531	0.792	0.531	0.542	0.613	0.495	0.767	0.520	0.549	0.549	0.517	0.514	0.500	0.497	0.548	0.520	0.532	0.645	0.541	0.525	0.527	0.545	0.534
amthyroid	0.676	0.777	0.789	0.788	0.608	0.816	0.761	0.453	0.710	0.918	0.889	0.676	0.548	0.735	0.631	0.453	0.599	0.966	0.814	0.781	0.923	0.964	0.603	0.864	0.642
backdoor	0.897	0.500	0.790	0.790	0.740	0.725	0.826	0.515	0.764	0.848	0.882	0.888	0.548	0.739	0.500	0.587	0.936	0.787	0.892	0.806	0.753	0.875	0.886	0.881	0.873
breastw	0.961	0.994	0.990	0.408	0.984	0.983	0.980	0.970	0.446	0.985	0.935	0.946	0.811	0.625	0.847	0.843	0.807	0.966	0.766	0.976	0.905	0.891	0.992	0.989	0.981
campain	0.738	0.783	0.769	0.594	0.768	0.738	0.740	0.750	0.446	0.775	0.737	0.734	0.581	0.508	0.500	0.445	0.766	0.566	0.724	0.746	0.660	0.789	0.727	0.746	0.725
cardio	0.832	0.921	0.935	0.579	0.839	0.922	0.830	0.856	0.551	0.815	0.934	0.949	0.625	0.498	0.655	0.908	0.461	0.796	0.723	0.777	0.631	0.721	0.911	0.714	0.857
cardiography	0.561	0.664	0.784	0.538	0.595	0.681	0.503	0.708	0.527	0.800	0.691	0.747	0.546	0.488	0.488	0.624	0.372	0.643	0.579	0.693	0.506	0.510	0.649	0.483	0.542
celeba	0.753	0.757	0.763	0.514	0.754	0.707	0.736	0.600	0.432	0.803	0.781	0.792	0.627	0.491	0.726	0.432	0.684	0.703	0.796	0.699	0.700	0.812	0.839	0.724	0.803
conus	0.664	0.800	0.500	0.538	0.611	0.807	0.671	0.454	0.562	0.731	0.655	0.944	0.742	0.527	0.447	0.488	0.668	0.604	0.659	0.672	0.629	0.646	0.665	0.702	0.662
cover	0.922	0.882	0.919	0.571	0.707	0.873	0.866	0.922	0.568	0.696	0.952	0.934	0.491	0.580	0.747	0.124	0.681	0.417	0.808	0.838	0.635	0.697	0.901	0.924	0.901
donors	0.808	0.815	0.888	0.691	0.743	0.829	0.566	0.629	0.765	0.770	0.825	0.558	0.511	0.511	0.747	0.225	0.739	0.899	0.806	0.832	0.796	0.785	0.813	0.810	0.601
fault	0.665	0.455	0.468	0.591	0.506	0.544	0.715	0.478	0.579	0.505	0.537	0.480	0.495	0.522	0.668	0.546	0.661	0.469	0.562	0.726	0.577	0.590	0.544	0.703	0.664
fraud	0.954	0.943	0.949	0.616	0.945	0.950	0.955	0.856	0.548	0.911	0.954	0.490	0.857	0.769	0.500	0.724	0.931	0.895	0.924	0.956	0.942	0.938	0.940	0.957	0.923
glass	0.855	0.760	0.710	0.659	0.820	0.790	0.870	0.624	0.618	0.795	0.604	0.715	0.630	0.517	0.743	0.545	0.729	0.766	0.560	0.881	0.681	0.864	0.708	0.812	0.771
hepatitis	0.635	0.807	0.737	0.469	0.768	0.683	0.669	0.557	0.468	0.721	0.704	0.840	0.681	0.582	0.637	0.637	0.616	0.654	0.461	0.631	0.451	0.577	0.781	0.674	0.804
http	0.996	0.991	0.980	0.288	0.991	1.000	0.951	0.060	0.338	1.000	0.994	0.997	0.838	0.249	0.500	0.996	0.921	0.994	0.998	0.051	0.973	0.995	0.995	0.994	0.996
intranets	0.616	0.676	0.677	0.494	0.696	0.686	0.616	0.541	0.587	0.660	0.615	0.888	0.719	0.451	0.779	0.414	0.658	0.782	0.749	0.849	0.852	0.656	0.618	0.690	0.743
ionosphere	0.892	0.783	0.717	0.876	0.544	0.833	0.922	0.788	0.864	0.951	0.838	0.777	0.641	0.514	0.766	0.829	0.629	0.884	0.758	0.924	0.697	0.911	0.768	0.922	0.857
landsat	0.548	0.422	0.368	0.540	0.575	0.474	0.614	0.382	0.549	0.607	0.423	0.366	0.533	0.631	0.626	0.306	0.649	0.464	0.496	0.602	0.473	0.544	0.457	0.571	0.538
letter	0.763	0.560	0.573	0.886	0.589	0.616	0.812	0.537	0.878	0.804	0.598	0.524	0.503	0.517	0.780	0.398	0.737	0.689	0.847	0.850	0.676	0.781	0.628	0.906	0.744
lymphography	0.994	0.996	0.995	0.523	0.995	0.999	0.995	0.900	0.636	0.989	0.996	0.997	0.840	0.681	0.878	0.995	0.884	0.940	0.958	0.809	0.852	0.834	1.000	0.987	0.991
magic gamma	0.725	0.681	0.638	0.700	0.709	0.721	0.795	0.655	0.678	0.699	0.673	0.667	0.584	0.604	0.728	0.442	0.676	0.742	0.763	0.801	0.872	0.765	0.728	0.829	0.743
magic gamma	0.795	0.681	0.638	0.700	0.709	0.721	0.795	0.655	0.678	0.699	0.673	0.667	0.584	0.604	0.728	0.442	0.676	0.742	0.763	0.801	0.872	0.765	0.728	0.829	0.743
magic gamma	0.795	0.681	0.638	0.700	0.709	0.721	0.795	0.655	0.678	0.699	0.673	0.667	0.584	0.604	0.728	0.442	0.676	0.742	0.763	0.801	0.872	0.765	0.728	0.829	0.743
magic gamma	0.795	0.681	0.638	0.700	0.709	0.721	0.795	0.655	0.678	0.699	0.673	0.667	0.584	0.604	0.728	0.442	0.676	0.742	0.763	0.801	0.872	0.765	0.728	0.829	0.743
magic gamma	0.795	0.681	0.638	0.700	0.709	0.721	0.795	0.655	0.678	0.699	0.673	0.667	0.584	0.604	0.728	0.442	0.676	0.742	0.763	0.801	0.872	0.765	0.728	0.829	0.743
magic gamma	0.795	0.681	0.638	0.700	0.709	0.721	0.795	0.655	0.678	0.699	0.673	0.667	0.584	0.604	0.728	0.442	0.676	0.742	0.763	0.801	0.872	0.765	0.728	0.829	0.743
magic gamma	0.795	0.681	0.638	0.700	0.709	0.721	0.795	0.655	0.678	0.699	0.673	0.667	0.584	0.604	0.728	0.442	0.676	0.742	0.763	0.801	0.872	0.765	0.728	0.829	0.743
magic gamma	0.795	0.681	0.638	0.700	0.709	0.721	0.795	0.655	0.678	0.699	0.673	0.667	0.584	0.604	0.728	0.442	0.676	0.742	0.763	0.801	0.872	0.765	0.728	0.829	0.743
magic gamma	0.795	0.681	0.638	0.700	0.709	0.721	0.795	0.655	0.678	0.699	0.673	0.667	0.584	0.604	0.728	0.442	0.676	0.742	0.763	0.801	0.872	0.765	0.728	0.829	0.743
magic gamma	0.795	0.681	0.638	0.700	0.709	0.721	0.795	0.655	0.678	0.699	0.673	0.667	0.584	0.604	0.728	0.442	0.676	0.742	0.763	0.801	0.872	0.765	0.728	0.829	0.743
magic gamma	0.795	0.681	0.638	0.700	0.709	0.721	0.795	0.655	0.678	0.699	0.673	0.667	0.584	0.604	0.728	0.442	0.676	0.742	0.763	0.801	0.872	0.765	0.728	0.829	0.743
magic gamma	0.795	0.681	0.638	0.700	0.709	0.721	0.795	0.655	0.678	0.699	0.673	0.667	0.584	0.604	0.728	0.442	0.676	0.742	0.763	0.801	0.872	0.765	0.728	0.829	0.743
magic gamma	0.795	0.681	0.638	0.700	0.709	0.721	0.795	0.655	0.678	0.699	0.673	0.667	0.584	0.604	0.728	0.442	0.676	0.742	0.763	0.801	0.872	0.765	0.728	0.829	0.743
magic gamma	0.795	0.681	0.638	0.700	0.709	0.721	0.795	0.655	0.678	0.699	0.673	0.667	0.584	0.604	0.728	0.442	0.676	0.742	0.763	0.801	0.872	0.765	0.728	0.829	0.743
magic gamma	0.795	0.681	0.638	0.700	0.709	0.721	0.795	0.655	0.678	0.699	0.673	0.667	0.584	0.604	0.728	0.442	0.676	0.742	0.763	0.801	0.872	0.765	0.728	0.829	0.743
magic gamma	0.795	0.681	0.638	0.700	0.709	0.721	0.795	0.655	0.678	0.699	0.673	0.667	0.584	0.604	0.728	0.442	0.676	0.742	0.763	0.801	0.872	0.765	0.728	0.829	0.743
magic gamma	0.795	0.681	0.638	0.700	0.709	0.721	0.795	0.655	0.678	0.699	0.673	0.667	0.584	0.604	0.728	0.442	0.676	0.742	0.763	0.801	0.872	0.765	0.728	0.829	0.743
magic gamma	0.795	0.681	0.638	0.700	0.709	0.721	0.795	0.655	0.678	0.699	0.673	0.667	0.584	0.604	0.728	0.442	0.676	0.742	0.763	0.801	0.872	0.765	0.728	0.829	0.743
magic gamma	0.795	0.681	0.638	0.700	0.709	0.721	0.795	0.655	0.678	0.699	0.673	0.667	0.584	0.604	0.728	0.442	0.676	0.742	0.763	0.801	0.872	0.765	0.728	0.829	0.743
magic gamma	0.795	0.681	0.638	0.700	0.709	0.721	0.795	0.655	0.678	0.699	0.673	0.667	0.584	0.604	0.728	0.442	0.676	0.742	0.763	0.801	0.872	0.765	0.728	0.829	0.743
magic gamma	0.795	0.681	0.638	0.700	0.709	0.721	0.795	0.655	0.678	0.699	0.673	0.667	0.584	0.604	0.728	0.442	0.676	0.742	0.763	0.801	0.872	0.765	0.728	0.829	0.743
magic gamma	0.795	0.681	0.638	0.700	0.709	0.721	0.795	0.655	0.678	0.699	0.673	0.667	0.584	0.604	0.728	0.442	0.676	0.742	0.763	0.801	0.872	0.765	0.728	0.829	0.743
magic gamma	0.795	0.681	0.638	0.700	0.709	0.721	0.795	0.655	0.678	0.699	0.673	0.667	0.584	0.604	0.728	0.442	0.676	0.742	0.763	0.801	0.872	0.765	0.728	0.829	0.743
magic gamma	0.795	0.681	0.638	0.700	0.709	0.721	0.795	0.655	0.678	0.699	0.673	0.667	0.584	0.604	0.728	0.442	0.676	0.742	0.763	0.801	0.872	0.765	0.728	0.829	0.743
magic gamma	0.795	0.681	0.638	0.700	0.709	0.721	0.795	0.655	0.678	0.699	0.673	0.667	0.584	0.604	0.728	0.442	0.676	0.742	0.763	0.801	0.872	0.765	0.728	0.829	0.743
magic gamma																									

	CBLOF	COPOD	ECOD	FeatureBagging	HBOS	IForest	kNN	LODA	LOF	MCD	OCSVM	PCA	DAGMM	DeepSVDD	DROCC	GOAD	ICL	PlanarFlow	DDPM	DTE-NP	DTE-IG	DTE-C	ODIM	ALTBI-G	ALTBI-I
aloi	0.037	0.031	0.033	0.104	0.034	0.034	0.048	0.033	0.097	0.032	0.039	0.037	0.033	0.034	0.030	0.033	0.046	0.032	0.036	0.056	0.040	0.033	0.040	0.037	0.036
amthyroid	0.169	0.174	0.272	0.206	0.228	0.312	0.224	0.098	0.163	0.503	0.188	0.196	0.109	0.192	0.186	0.131	0.123	0.654	0.297	0.228	0.380	0.670	0.166	0.350	0.156
backdoor	0.547	0.025	0.025	0.217	0.052	0.045	0.279	0.101	0.358	0.122	0.534	0.250	0.531	0.372	0.025	0.479	0.717	0.336	0.520	0.473	0.438	0.481	0.406	0.128	0.150
breastw	0.890	0.989	0.982	0.284	0.954	0.956	0.932	0.955	0.927	0.962	0.897	0.946	0.660	0.482	0.776	0.826	0.635	0.908	0.537	0.921	0.770	0.715	0.982	0.966	0.944
campain	0.287	0.368	0.354	0.145	0.352	0.279	0.289	0.131	0.158	0.325	0.283	0.284	0.163	0.149	0.113	0.105	0.267	0.191	0.299	0.281	0.237	0.321	0.315	0.333	0.247
cardio	0.482	0.576	0.567	0.161	0.458	0.559	0.402	0.428	0.159	0.364	0.536	0.609	0.193	0.177	0.272	0.540	0.108	0.471	0.278	0.376	0.184	0.268	0.526	0.386	0.521
cardiotocography	0.335	0.403	0.502	0.276	0.361	0.436	0.324	0.463	0.272	0.311	0.408	0.462	0.271	0.252	0.258	0.403	0.188	0.348	0.338	0.312	0.250	0.276	0.422	0.337	0.419
celeba	0.069	0.093	0.095	0.024	0.090	0.063	0.061	0.047	0.112	0.092	0.103	0.112	0.044	0.031	0.047	0.021	0.045	0.066	0.093	0.052	0.058	0.077	0.123	0.061	0.092
conus	0.088	0.062	0.062	0.061	0.073	0.073	0.088	0.065	0.069	0.153	0.085	0.087	0.062	0.075	0.058	0.072	0.095	0.074	0.086	0.090	0.083	0.081	0.089	0.089	0.089
cover	0.070	0.068	0.113	0.019	0.026	0.052	0.054	0.090	0.019	0.016	0.099	0.075	0.044	0.048	0.056	0.005	0.022	0.010	0.046	0.040	0.025	0.021	0.068	0.178	0.050
donors	0.148	0.209	0.265	0.120	0.135	0.124	0.182	0.255	0.109	0.141	0.139	0.166	0.086	0.112	0.123	0.040	0.119	0.241	0.143	0.188	0.164	0.140	0.136	0.140	0.072
fault	0.473	0.313	0.325	0.306	0.360	0.395	0.522	0.337	0.388	0.334	0.401	0.332	0.361	0.375	0.496	0.381	0.473	0.329	0.392	0.532	0.417	0.422	0.412	0.512	0.474
frand	0.175	0.252	0.215	0.003	0.209	0.145	0.169	0.146	0.033	0.488	0.110	0.149	0.084	0.250	0.002	0.257	0.127	0.447	0.146	0.152	0.188	0.648	0.369	0.334	0.346
glass	0.144	0.111	0.183	0.151	0.161	0.144	0.167	0.090	0.144	0.113	0.130	0.112	0.111	0.090	0.159	0.076	0.122	0.113	0.073	0.206	0.135	0.168	0.161	0.111	0.095
hepatitis	0.304	0.389	0.295	0.225	0.328	0.243	0.252	0.275	0.214	0.363	0.277	0.339	0.253	0.170	0.221	0.199	0.231	0.317	0.165	0.238	0.215	0.257	0.319	0.259	0.430
http	0.464	0.280	0.145	0.047	0.302	0.886	0.010	0.004	0.050	0.865	0.556	0.500	0.368	0.093	0.004	0.441	0.091	0.363	0.642	0.024	0.295	0.440	0.259	0.222	0.294
intranetads	0.297	0.505	0.505	0.182	0.523	0.486	0.296	0.242	0.232	0.344	0.291	0.276	0.207	0.252	0.197	0.288	0.237	0.262	0.295	0.290	0.275	0.302	0.281	0.500	0.354
ionosphere	0.881	0.663	0.633	0.821	0.353	0.779	0.911	0.741	0.807	0.947	0.829	0.721	0.473	0.392	0.728	0.781	0.472	0.824	0.633	0.920	0.610	0.880	0.700	0.911	0.814
landsat	0.212	0.176	0.164	0.246	0.231	0.194	0.238	0.183	0.250	0.253	0.175	0.165	0.230	0.362	0.272	0.198	0.329	0.187	0.200	0.255	0.181	0.223	0.181	0.241	0.210
letter	0.166	0.068	0.077	0.445	0.078	0.086	0.203	0.083	0.433	0.174	0.113	0.076	0.083	0.099	0.252	0.059	0.208	0.153	0.367	0.255	0.181	0.257	0.088	0.395	0.130
lymphography	0.915	0.907	0.894	0.090	0.919	0.972	0.894	0.491	0.135	0.767	0.885	0.935	0.454	0.254	0.463	0.897	0.264	0.417	0.731	0.805	0.388	0.381	1.000	0.705	0.780
magic gamma	0.666	0.588	0.533	0.539	0.617	0.638	0.724	0.579	0.520	0.632	0.625	0.589	0.450	0.499	0.627	0.326	0.548	0.692	0.651	0.730	0.657	0.664	0.650	0.767	0.685
magic gamma	0.140	0.430	0.435	0.070	0.132	0.218	0.181	0.218	0.085	0.036	0.187	0.204	0.111	0.025	0.114	0.046	0.046	0.074	0.099	0.175	0.082	0.170	0.086	0.163	0.068
mammography	1.000	0.369	0.475	0.140	0.999	0.945	0.708	0.842	0.118	0.992	1.000	1.000	0.500	0.107	0.196	1.000	0.128	0.391	0.984	0.434	0.137	0.553	1.000	1.000	1.000
mask	0.059	0.029	0.029	0.036	0.192	0.046	0.022	0.029	0.035	0.022	0.027	0.027	0.026	0.039	0.032	0.039	0.030	0.027	0.022	0.021	0.028	0.028	0.029	0.029	0.039
optdigits	0.547	0.370	0.520	0.341	0.319	0.464	0.556	0.410	0.292	0.617	0.531	0.525	0.255	0.288	0.632	0.373	0.285	0.538	0.493	0.530	0.507	0.555	0.503	0.467	0.554
pageblocks	0.192	0.177	0.270	0.048	0.247	0.260	0.100	0.186	0.400	0.069	0.226	0.219	0.056	0.022	0.027	0.075	0.045	0.060	0.056	0.089	0.044	0.044	0.236	0.116	0.188
pendigits	0.402	0.045	0.589	0.001	0.518	0.488	0.415	0.387	0.360	0.349	0.402	0.409	0.389	0.456	0.383	0.387	0.370	0.433	0.384	0.407	0.399	0.400	0.408	0.485	0.388
spambase	0.019	0.019	0.020	0.022	0.023	0.021	0.019	0.016	0.022	0.019	0.019	0.018	0.022	0.018	0.020	0.019	0.020	0.018	0.020	0.019	0.019	0.020	0.020	0.018	0.017
speed	0.211	0.398	0.324	0.143	0.332	0.347	0.317	0.280	0.153	0.257	0.318	0.364	0.198	0.099	0.241	0.285	0.117	0.284	0.143	0.273	0.235	0.226	0.355	0.196	0.317
stamps	0.272	0.179	0.472	0.069	0.501	0.562	0.392	0.189	0.077	0.702	0.329	0.356	0.126	0.024	0.338	0.318	0.066	0.734	0.325	0.360	0.118	0.705	0.244	0.452	0.225
thyroid	0.123	0.085	0.110	0.124	0.091	0.097	0.095	0.089	0.130	0.101	0.107	0.099	0.134	0.107	0.118	0.124	0.115	0.111	0.150	0.098	0.133	0.119	0.153	0.090	0.103
vertebral	0.166	0.034	0.083	0.314	0.078	0.162	0.443	0.127	0.326	0.085	0.196	0.069	0.041	0.037	0.178	0.154	0.219	0.295	0.311	0.504	0.166	0.417	0.255	0.521	0.210
vowels	0.314	0.308	0.332	0.326	0.328	0.304	0.294	0.330	0.315	0.298	0.303	0.302	0.353	0.340	0.284	0.332	0.318	0.309	0.320	0.295	0.306	0.306	0.292	0.305	0.299
waveform	0.122	0.057	0.040	0.078	0.048	0.056	0.133	0.040	0.071	0.040	0.052	0.044	0.032	0.061	0.150	0.042	0.063	0.150	0.050	0.109	0.037	0.043	0.060	0.061	0.101
wbc	0.691	0.883	0.882	0.037	0.728	0.948	0.743	0.898	0.077	0.839	0.813	0.913	0.327	0.069	0.358	0.736	0.211	0.431	0.758	0.722	0.348	0.194	1.000	0.679	0.902
wbc	0.688	0.760	0.493	0.155	0.761	0.702	0.521	0.527	0.128	0.395	0.539	0.613	0.152	0.063	0.039	0.589	0.065	0.568	0.483	0.465	0.074	0.157	0.393	0.290	0.568
wdbc	0.688	0.760	0.493	0.155	0.761	0.702	0.521	0.527	0.128	0.395	0.539	0.613	0.152	0.063	0.039	0.589	0.065	0.568	0.483	0.465	0.074	0.157	0.393	0.290	0.568
wilt	0.040	0.037	0.042	0.081	0.039	0.044	0.049	0.036	0.083	0.153	0.035	0.032	0.047	0.046	0.041	0.065	0.109	0.115	0.076	0.054	0.211	0.163	0.036	0.071	0.037
wine	0.170	0.364	0.195	0.061	0.412	0.207	0.081	0.250	0.064	0.737	0.155	0.264	0.120	0.116	0.126	0.229	0.087	0.086	0.075	0.074	0.064	0.103	0.335	0.219	0.385
wdbc	0.227	0.364	0.195	0.061	0.412	0.207	0.081	0.250	0.064	0.737	0.155	0.264	0.120	0.116	0.126	0.229	0.087	0.086	0.075	0.074	0.064	0.103	0.335	0.219	0.385
wpbc	0.227	0.364	0.195	0.061	0.412	0.207	0.081	0.250	0.064	0.737	0.155	0.264	0.120	0.116	0.126	0.229	0.087	0.086	0.075	0.074	0.064	0.103	0.335	0.219	0.385
yeast	0.314	0.308	0.332	0.326	0.328	0.304	0.294	0.330	0.315	0.298	0.303	0.302	0.353	0.340	0.284	0.332	0.318	0.309	0.320	0.295	0.306	0.306	0.292	0.305	0.299
CIFAR10	0.103	0.065	0.067	0.115	0.075	0.089	0.102	0.086	0.115	0.084	0.102	0.101	0.062	0.073	0.060	0.102	0.070	0.085	0.102	0.104	0.078	0.092	0.557	0.499	0.531
MNIST-C	0.173	0.050	0.050	0.128	0.126	0.178	0.191	0.101	0.127	0.166	0.179	0.101	0.062	0.097	0.096	0.177	0.098	0.154	0.178	0.192	0.141	0.157	0.281	0.281	0.305
MVTec-AD	0.570	0.236	0.236	0.536	0.546	0.570	0.580	0.464	0.532	0.451	0.555	0.540	0.362	0.387	0.317	0.546	0.404	0.454	0.546	0.578	0.439	0.517	0.738	0.444	0.560
SVHN	0																								

	CBLOF	COPOD	ECOD	FeatureBagging	HBOS	iForest	KNN	LODA	LOF	MCD	OC5VM	PCA	DAGMM	DeepSVDD	DR OCC	GOAD	ICL	PlanarFlow	DDPM	DTE-NP	DTE-IG	DTE-C	ALTBI
aloi	0.537	0.495	0.517	0.491	0.522	0.507	0.510	0.492	0.488	0.485	0.543	0.540	0.508	0.509	0.500	0.480	0.475	0.485	0.499	0.512	0.509	0.504	0.539
amthyroid	0.901	0.768	0.785	0.890	0.660	0.903	0.928	0.774	0.886	0.902	0.885	0.852	0.722	0.550	0.889	0.810	0.811	0.932	0.888	0.929	0.876	0.975	0.655
backdoor	0.697	0.500	0.500	0.948	0.708	0.749	0.938	0.476	0.953	0.851	0.625	0.646	0.544	0.911	0.943	0.529	0.936	0.760	0.809	0.933	0.940	0.917	0.927
breastw	0.991	0.995	0.991	0.591	0.992	0.995	0.991	0.981	0.889	0.987	0.994	0.992	0.895	0.970	0.473	0.989	0.983	0.979	0.987	0.983	0.787	0.928	0.982
campaign	0.771	0.782	0.769	0.691	0.771	0.736	0.785	0.589	0.706	0.785	0.777	0.771	0.615	0.622	0.500	0.479	0.809	0.698	0.745	0.788	0.748	0.780	0.749
cardio	0.935	0.932	0.950	0.921	0.807	0.933	0.920	0.913	0.922	0.828	0.956	0.965	0.779	0.654	0.621	0.960	0.800	0.889	0.869	0.918	0.738	0.873	0.869
cardiography	0.676	0.664	0.793	0.636	0.612	0.742	0.621	0.728	0.645	0.571	0.752	0.789	0.671	0.478	0.462	0.761	0.542	0.699	0.545	0.638	0.524	0.601	0.686
celeba	0.793	0.757	0.763	0.469	0.767	0.712	0.621	0.625	0.437	0.844	0.798	0.805	0.638	0.562	0.689	0.438	0.722	0.716	0.786	0.704	0.822	0.701	0.701
conus	0.708	0.500	0.500	0.559	0.625	0.626	0.723	0.511	0.858	0.741	0.700	0.744	0.529	0.542	0.554	0.352	0.706	0.352	0.706	0.702	0.618	0.696	0.704
cover	0.940	0.882	0.919	0.992	0.711	0.863	0.975	0.949	0.992	0.700	0.962	0.944	0.752	0.491	0.958	0.138	0.893	0.475	0.984	0.977	0.958	0.978	0.947
donors	0.935	0.815	0.887	0.952	0.812	0.894	0.995	0.635	0.970	0.819	0.921	0.881	0.622	0.730	0.742	0.336	0.999	0.916	0.825	0.993	0.993	0.982	0.960
donors	0.935	0.815	0.887	0.952	0.812	0.894	0.995	0.635	0.970	0.819	0.921	0.881	0.622	0.730	0.742	0.336	0.999	0.916	0.825	0.993	0.993	0.982	0.960
donors	0.935	0.815	0.887	0.952	0.812	0.894	0.995	0.635	0.970	0.819	0.921	0.881	0.622	0.730	0.742	0.336	0.999	0.916	0.825	0.993	0.993	0.982	0.960
donors	0.935	0.815	0.887	0.952	0.812	0.894	0.995	0.635	0.970	0.819	0.921	0.881	0.622	0.730	0.742	0.336	0.999	0.916	0.825	0.993	0.993	0.982	0.960
donors	0.935	0.815	0.887	0.952	0.812	0.894	0.995	0.635	0.970	0.819	0.921	0.881	0.622	0.730	0.742	0.336	0.999	0.916	0.825	0.993	0.993	0.982	0.960
donors	0.935	0.815	0.887	0.952	0.812	0.894	0.995	0.635	0.970	0.819	0.921	0.881	0.622	0.730	0.742	0.336	0.999	0.916	0.825	0.993	0.993	0.982	0.960
donors	0.935	0.815	0.887	0.952	0.812	0.894	0.995	0.635	0.970	0.819	0.921	0.881	0.622	0.730	0.742	0.336	0.999	0.916	0.825	0.993	0.993	0.982	0.960
donors	0.935	0.815	0.887	0.952	0.812	0.894	0.995	0.635	0.970	0.819	0.921	0.881	0.622	0.730	0.742	0.336	0.999	0.916	0.825	0.993	0.993	0.982	0.960
donors	0.935	0.815	0.887	0.952	0.812	0.894	0.995	0.635	0.970	0.819	0.921	0.881	0.622	0.730	0.742	0.336	0.999	0.916	0.825	0.993	0.993	0.982	0.960
donors	0.935	0.815	0.887	0.952	0.812	0.894	0.995	0.635	0.970	0.819	0.921	0.881	0.622	0.730	0.742	0.336	0.999	0.916	0.825	0.993	0.993	0.982	0.960
donors	0.935	0.815	0.887	0.952	0.812	0.894	0.995	0.635	0.970	0.819	0.921	0.881	0.622	0.730	0.742	0.336	0.999	0.916	0.825	0.993	0.993	0.982	0.960
donors	0.935	0.815	0.887	0.952	0.812	0.894	0.995	0.635	0.970	0.819	0.921	0.881	0.622	0.730	0.742	0.336	0.999	0.916	0.825	0.993	0.993	0.982	0.960
donors	0.935	0.815	0.887	0.952	0.812	0.894	0.995	0.635	0.970	0.819	0.921	0.881	0.622	0.730	0.742	0.336	0.999	0.916	0.825	0.993	0.993	0.982	0.960
donors	0.935	0.815	0.887	0.952	0.812	0.894	0.995	0.635	0.970	0.819	0.921	0.881	0.622	0.730	0.742	0.336	0.999	0.916	0.825	0.993	0.993	0.982	0.960
donors	0.935	0.815	0.887	0.952	0.812	0.894	0.995	0.635	0.970	0.819	0.921	0.881	0.622	0.730	0.742	0.336	0.999	0.916	0.825	0.993	0.993	0.982	0.960
donors	0.935	0.815	0.887	0.952	0.812	0.894	0.995	0.635	0.970	0.819	0.921	0.881	0.622	0.730	0.742	0.336	0.999	0.916	0.825	0.993	0.993	0.982	0.960
donors	0.935	0.815	0.887	0.952	0.812	0.894	0.995	0.635	0.970	0.819	0.921	0.881	0.622	0.730	0.742	0.336	0.999	0.916	0.825	0.993	0.993	0.982	0.960
donors	0.935	0.815	0.887	0.952	0.812	0.894	0.995	0.635	0.970	0.819	0.921	0.881	0.622	0.730	0.742	0.336	0.999	0.916	0.825	0.993	0.993	0.982	0.960
donors	0.935	0.815	0.887	0.952	0.812	0.894	0.995	0.635	0.970	0.819	0.921	0.881	0.622	0.730	0.742	0.336	0.999	0.916	0.825	0.993	0.993	0.982	0.960
donors	0.935	0.815	0.887	0.952	0.812	0.894	0.995	0.635	0.970	0.819	0.921	0.881	0.622	0.730	0.742	0.336	0.999	0.916	0.825	0.993	0.993	0.982	0.960
donors	0.935	0.815	0.887	0.952	0.812	0.894	0.995	0.635	0.970	0.819	0.921	0.881	0.622	0.730	0.742	0.336	0.999	0.916	0.825	0.993	0.993	0.982	0.960
donors	0.935	0.815	0.887	0.952	0.812	0.894	0.995	0.635	0.970	0.819	0.921	0.881	0.622	0.730	0.742	0.336	0.999	0.916	0.825	0.993	0.993	0.982	0.960
donors	0.935	0.815	0.887	0.952	0.812	0.894	0.995	0.635	0.970	0.819	0.921	0.881	0.622	0.730	0.742	0.336	0.999	0.916	0.825	0.993	0.993	0.982	0.960
donors	0.935	0.815	0.887	0.952	0.812	0.894	0.995	0.635	0.970	0.819	0.921	0.881	0.622	0.730	0.742	0.336	0.999	0.916	0.825	0.993	0.993	0.982	0.960
donors	0.935	0.815	0.887	0.952	0.812	0.894	0.995	0.635	0.970	0.819	0.921	0.881	0.622	0.730	0.742	0.336	0.999	0.916	0.825	0.993	0.993	0.982	0.960
donors	0.935	0.815	0.887	0.952	0.812	0.894	0.995	0.635	0.970	0.819	0.921	0.881	0.622	0.730	0.742	0.336	0.999	0.916	0.825	0.993	0.993	0.982	0.960
donors	0.935	0.815	0.887	0.952	0.812	0.894	0.995	0.635	0.970	0.819	0.921	0.881	0.622	0.730	0.742	0.336	0.999	0.916	0.825	0.993	0.993	0.982	0.960
donors	0.935	0.815	0.887	0.952	0.812	0.894	0.995	0.635	0.970	0.819	0.921	0.881	0.622	0.730	0.742	0.336	0.999	0.916	0.825	0.993	0.993	0.982	0.960
donors	0.935	0.815	0.887	0.952	0.812	0.894	0.995	0.635	0.970	0.819	0.921	0.881	0.622	0.730	0.742	0.336	0.999	0.916	0.825	0.993	0.993	0.982	0.960
donors	0.935	0.815	0.887	0.952	0.812	0.894	0.995	0.635	0.970	0.819	0.921	0.881	0.622	0.730	0.742	0.336	0.999	0.916	0.825	0.993	0.993	0.982	0.960
donors	0.935	0.815	0.887	0.952	0.812	0.894	0.995	0.635	0.970	0.819	0.921	0.881	0.622	0.730	0.742	0.336	0.999	0.916	0.825	0.993	0.993	0.982	0.960
donors	0.935	0.815	0.887	0.952	0.812	0.894	0.995	0.635	0.970	0.819	0.921	0.881	0.622	0.730	0.742	0.336	0.999	0.916	0.825	0.993	0.993	0.982	0.960
donors	0.935	0.815	0.887	0.952	0.812	0.894	0.995	0.635	0.970	0.819	0.921	0.881	0.622	0.730	0.742	0.336	0.999	0.916	0.825	0.993	0.993	0.982	0.960
donors	0.935	0.815	0.887	0.952	0.812	0.894	0.995	0.635	0.970	0.819	0.921	0.881	0.622	0.730	0.742	0.336	0.999	0.916	0.825	0.993	0.993	0.982	0.960
donors	0.935	0.815	0.887	0.952	0.812	0.894	0.995	0.635	0.970	0.819	0.921	0.881	0.622	0.730	0.742	0.336	0.999	0.916	0.825	0.993	0.993	0.982	0.960
donors	0.935	0.815	0.887	0.952	0.812	0.894	0.995	0.635	0.970	0.819	0.921	0.881	0.622	0.730	0.742	0.336	0.999	0.916	0.825	0.993	0.993	0.982	0.960
donors	0.935	0.815	0.887	0.952	0.812	0.894	0.995	0.635	0.970	0.819	0.921	0.881	0.622	0.730	0.742	0.336	0.999	0.916	0.825	0.993	0.993	0.982	0.960
donors	0.935	0.815	0.887	0.952	0.812	0.894	0.995	0.635	0.970	0.819	0.921	0.881	0.622	0.730	0.742	0.336	0.999	0.916	0.825	0.993	0.993	0.982	0.960
donors	0.935	0.815	0.887	0.952	0.812	0.894	0.995	0.635	0.970	0.819	0.921	0.881	0.622	0.730	0.742	0.336	0.999	0.916	0.825	0.993	0.993	0.982	0.960
donors	0.935	0.815	0.887	0.952	0.812	0.894	0.995	0.635	0.970	0.819	0.921	0.881	0.622	0.730	0.742	0.336	0.999	0.916	0.825	0.993	0.993	0	

	CBLOF	COPOD	ECOD	FeatureBagging	HBOS	iForest	KNN	LODA	LOF	MCD	OCSVM	PCA	DAGMM	DeepSVDD	DR OCC	GOAD	ICL	PlanarFlow	DDPM	DTE-NP	DTE-IG	DTE-C	ALTBI
aloi	0.064	0.057	0.061	0.068	0.064	0.058	0.060	0.059	0.065	0.056	0.065	0.065	0.061	0.062	0.059	0.057	0.055	0.055	0.060	0.061	0.060	0.058	0.040
amthyroid	0.636	0.296	0.400	0.485	0.390	0.594	0.681	0.460	0.535	0.597	0.601	0.566	0.480	0.478	0.637	0.587	0.458	0.652	0.629	0.499	0.499	0.829	0.207
backdoor	0.091	0.048	0.048	0.495	0.086	0.094	0.465	0.060	0.353	0.222	0.077	0.079	0.075	0.248	0.846	0.067	0.892	0.322	0.142	0.457	0.820	0.624	0.815
breastw	0.991	0.994	0.992	0.524	0.497	0.957	0.989	0.968	0.800	0.983	0.994	0.992	0.910	0.960	0.632	0.088	0.968	0.975	0.986	0.902	0.814	0.883	0.960
campaign	0.486	0.511	0.495	0.333	0.497	0.457	0.490	0.298	0.402	0.479	0.494	0.488	0.324	0.370	0.203	0.231	0.489	0.428	0.489	0.500	0.462	0.469	0.340
cardio	0.809	0.749	0.786	0.716	0.589	0.786	0.772	0.725	0.702	0.671	0.836	0.862	0.559	0.389	0.512	0.848	0.479	0.689	0.693	0.774	0.411	0.693	0.530
cardiologography	0.617	0.561	0.690	0.570	0.507	0.629	0.574	0.606	0.573	0.528	0.662	0.697	0.597	0.458	0.439	0.675	0.487	0.593	0.513	0.587	0.396	0.533	0.490
celeba	0.185	0.165	0.169	0.039	0.168	0.117	0.119	0.095	0.056	0.190	0.203	0.210	0.090	0.071	0.077	0.040	0.097	0.129	0.180	0.107	0.134	0.142	0.042
convs	0.203	0.117	0.117	0.120	0.140	0.142	0.121	0.134	0.137	0.290	0.203	0.200	0.132	0.154	0.143	0.087	0.212	0.147	0.197	0.163	0.179	0.106	0.106
cover	0.160	0.123	0.192	0.082	0.054	0.087	0.558	0.226	0.829	0.031	0.223	0.162	0.098	0.027	0.133	0.011	0.345	0.020	0.733	0.600	0.804	0.637	0.227
donors	0.465	0.335	0.413	0.653	0.363	0.405	0.901	0.254	0.634	0.312	0.427	0.352	0.195	0.428	0.302	0.090	0.984	0.493	0.267	0.856	0.958	0.713	0.433
fault	0.613	0.532	0.517	0.508	0.539	0.592	0.620	0.545	0.504	0.634	0.611	0.604	0.568	0.555	0.578	0.621	0.632	0.604	0.648	0.622	0.638	0.639	0.560
fraud	0.278	0.384	0.332	0.631	0.323	0.182	0.387	0.366	0.351	0.601	0.296	0.269	0.156	0.483	0.003	0.294	0.539	0.628	0.692	0.421	0.311	0.621	0.354
glass	0.317	0.201	0.250	0.361	0.276	0.214	0.423	0.156	0.381	0.203	0.268	0.210	0.186	0.524	0.231	0.183	0.924	0.309	0.312	0.374	0.806	0.415	0.362
hepatitis	0.634	0.561	0.458	0.446	0.635	0.554	0.903	0.502	0.437	0.568	0.776	0.649	0.544	0.987	0.349	0.658	0.998	0.896	0.951	0.823	0.998	0.958	0.239
http	0.903	0.463	0.252	0.082	0.390	0.534	1.000	0.075	0.971	0.922	0.999	0.917	0.575	0.361	0.007	0.684	0.708	0.522	1.000	0.971	0.788	0.555	0.233
inmternads	0.470	0.617	0.619	0.493	0.308	0.292	0.492	0.393	0.504	0.344	0.482	0.470	0.318	0.516	0.431	0.474	0.600	0.476	0.477	0.513	0.587	0.552	0.820
ionosphere	0.973	0.785	0.756	0.949	0.646	0.917	0.980	0.852	0.946	0.967	0.975	0.909	0.775	0.981	0.717	0.932	0.991	0.976	0.964	0.982	0.969	0.968	0.910
landstar	0.369	0.338	0.311	0.615	0.601	0.473	0.549	0.357	0.614	0.397	0.370	0.320	0.403	0.494	0.376	0.312	0.531	0.342	0.348	0.545	0.327	0.368	0.276
letter	0.083	0.089	0.107	0.117	0.087	0.082	0.080	0.113	0.081	0.083	0.080	0.080	0.104	0.089	0.157	0.081	0.128	0.092	0.095	0.086	0.102	0.090	0.200
lymphography	0.983	0.939	0.944	0.727	0.966	0.944	0.992	0.241	0.842	0.868	1.000	0.985	0.735	0.968	0.309	0.988	1.000	0.962	0.993	0.993	0.998	0.868	0.917
magic_gamma	0.802	0.722	0.679	0.869	0.772	0.803	0.859	0.758	0.864	0.772	0.992	0.782	0.645	0.695	0.832	0.761	0.813	0.785	0.880	0.887	0.887	0.897	0.771
magic_gamma	0.411	0.546	0.552	0.293	0.213	0.379	0.413	0.432	0.341	0.080	0.405	0.417	0.220	0.275	0.272	0.278	0.171	0.185	0.199	0.421	0.334	0.398	0.242
magic_gamma	1.000	0.961	0.982	1.000	1.000	1.000	1.000	1.000	1.000	0.663	1.000	1.000	1.000	0.999	0.999	1.000	0.922	0.327	1.000	1.000	0.889	1.000	1.000
magic_gamma	0.140	0.056	0.056	0.412	0.424	0.154	0.291	0.039	0.456	0.071	0.069	0.060	0.050	0.045	0.192	0.078	0.509	0.039	0.256	0.318	0.221	0.153	0.119
magic_gamma	0.706	0.415	0.585	0.702	0.423	0.434	0.676	0.486	0.711	0.632	0.643	0.594	0.603	0.521	0.735	0.635	0.681	0.583	0.521	0.575	0.575	0.664	0.671
magic_gamma	0.512	0.309	0.415	0.857	0.425	0.588	0.970	0.372	0.786	0.132	0.518	0.386	0.117	0.093	0.146	0.334	0.664	0.145	0.611	0.919	0.592	0.484	0.283
magic_gamma	0.721	0.691	0.648	0.695	0.759	0.737	0.754	0.594	0.684	0.686	0.720	0.712	0.565	0.598	0.598	0.652	0.786	0.712	0.797	0.696	0.680	0.563	0.563
magic_gamma	0.773	0.733	0.696	0.858	0.865	0.824	0.860	0.798	0.859	0.799	0.809	0.778	0.760	0.811	0.775	0.790	0.876	0.779	0.851	0.858	0.817	0.848	0.755
magic_gamma	0.968	0.853	0.797	0.907	0.877	0.945	0.967	0.937	0.885	0.983	0.969	0.919	0.475	0.763	0.793	0.959	0.947	0.625	0.881	0.962	0.833	0.682	0.969
magic_gamma	0.968	0.981	0.952	0.464	0.975	0.986	0.979	0.557	0.998	0.909	0.977	0.963	0.660	0.980	0.134	0.602	0.997	0.517	0.979	0.981	0.994	0.940	0.244
magic_gamma	0.695	0.297	0.305	0.492	0.534	0.646	0.982	0.530	0.617	0.624	0.663	0.364	0.504	0.430	0.656	0.422	0.325	0.747	0.764	0.948	0.969	0.691	0.571
magic_gamma	0.497	0.010	0.680	0.004	0.012	0.011	0.505	0.082	0.441	0.012	0.645	0.495	0.209	0.307	0.079	0.324	0.038	0.008	0.408	0.502	0.336	0.504	0.353
magic_gamma	0.820	0.736	0.713	0.684	0.784	0.883	0.833	0.802	0.727	0.818	0.822	0.818	0.742	0.753	0.791	0.821	0.868	0.854	0.729	0.837	0.810	0.838	0.543
magic_gamma	0.027	0.028	0.029	0.030	0.032	0.033	0.028	0.030	0.032	0.028	0.028	0.028	0.040	0.034	0.034	0.028	0.034	0.033	0.030	0.032	0.029	0.029	0.017
magic_gamma	0.622	0.564	0.490	0.656	0.523	0.588	0.717	0.572	0.648	0.417	0.649	0.588	0.465	0.426	0.285	0.496	0.795	0.524	0.647	0.825	0.728	0.577	0.613
magic_gamma	0.815	0.302	0.640	0.365	0.770	0.797	0.809	0.643	0.606	0.801	0.789	0.813	0.631	0.691	0.744	0.801	0.515	0.758	0.822	0.810	0.457	0.817	0.398
magic_gamma	0.252	0.155	0.199	0.329	0.189	0.208	0.261	0.167	0.339	0.210	0.222	0.193	0.251	0.234	0.234	0.214	0.588	0.230	0.358	0.252	0.515	0.351	0.090
magic_gamma	0.448	0.382	0.326	0.410	0.426	0.407	0.461	0.383	0.412	0.452	0.409	0.400	0.372	0.749	0.132	0.209	0.274	0.097	0.427	0.316	0.336	0.381	0.499
magic_gamma	0.507	0.468	0.494	0.499	0.498	0.468	0.483	0.490	0.489	0.457	0.480	0.468	0.518	0.492	0.498	0.508	0.496	0.470	0.511	0.481	0.511	0.497	0.323
magic_gamma	0.197	0.121	0.126	0.222	0.140	0.165	0.196	0.169	0.222	0.159	0.194	0.192	0.120	0.140	0.124	0.194	0.174	0.159	0.196	0.199	0.167	0.197	0.693
magic_gamma	0.425	0.095	0.095	0.222	0.216	0.328	0.462	0.326	0.519	0.258	0.416	0.403	0.234	0.314	0.269	0.412	0.515	0.341	0.418	0.474	0.441	0.472	0.506
magic_gamma	0.749	0.378	0.378	0.758	0.676	0.700	0.738	0.657	0.758	0.805	0.730	0.721	0.581	0.838	0.593	0.726	0.895	0.679	0.737	0.829	0.829	0.851	0.806
magic_gamma	0.151	0.095	0.095	0.161	0.120	0.139	0.153	0.127	0.160	0.128	0.150	0.149	0.114	0.160	0.112	0.149	0.136	0.142	0.151	0.155	0.142	0.155	0.077
magic_gamma	0.665	0.169	0.169	0.693	0.222	0.542	0.727	0.341	0.710	0.558	0.662	0.650	0.461	0.460	0.597	0.651	0.685	0.552	0.624	0.737	0.561	0.563	0.991
magic_gamma	0.578	0.095	0.095	0.639	0.349	0.447	0.592	0.469	0.636	0.374	0.565	0.562	0.297	0.451	0.296	0.566	0.631	0.468	0.571	0.598	0.537	0.550	0.989
magic_gamma	0.126	0.111	0.113	0.150	0.111	0.116	0.135	0.112	0.150	0.155	0.113	0.113	0.113	0.129	0.120	0.120	0.115	0.146	0.106	0.115	0.156	0.173	0.241
magic_gamma	0.138	0.111	0.109	0.259	0.112	0.119	0.167	0.121	0.259	0.146	0.128	0.116	0.102	0.102	0.097	0.124	0.154	0.097	0.119	0.117	0.128	0.192	0.367
magic_gamma	0.115	0.112	0.104	0.111	0.111	0.111	0.111	0.102	0.110	0.117	0.111	0.107	0.095	0.102	0.095	0.109	0.102	0.096	0.108	0.117	0.101	0.112	0.061
magic_gamma	0.090	0.093	0.085	0.090	0.090	0.090	0.089	0.087	0.090	0.095	0.089	0.087	0.092	0.097	0.099	0.088	0.102	0.095	0.087	0.090	0.101	0	

B.4. Ablation studies

The optimal loss usage percentage We examine the optimal amount of loss truncation required when implementing ALTBI. The table shows the averaged AUC on `ADBench` datasets for various loss usage percentages. We can identify that using 92 percent of loss values performs best in our method.

ρ	0.90	0.92	0.94	0.96	0.98	1.00
AUC	0.759	0.762	0.759	0.758	0.756	0.755

Table B.6. Averaged results of training AUC scores with various values of ρ .

The increase in mini-batch sizes We investigate how much to increase the mini-batch size at each update for optimal performance. There was no significant difference in scores with varying γ values, but the highest score was achieved with a γ of 1.03. Therefore, we chose this value for our experiments.

γ	1.00	1.01	1.02	1.03	1.04	1.05	1.07	1.1
AUC	0.761	0.760	0.761	0.762	0.761	0.762	0.761	0.761

Table B.7. Averaged results of training AUC scores with various values of γ

Number of samples used in the IWAE Table B.8 shows the averaged AUC values on 57 `ADBench` datasets with various numbers of samples in the IWAE ranging from 1 to 100. It should be noted that $K=1$ is equivalent to the original VAE. We observe that as the value of K increases, the scores decline and then stabilize. Therefore, we choose $K=2$ in our experiments.

K	1	2	5	10	20	50	70	100
AUC	0.760	0.762	0.755	0.760	0.759	0.758	0.753	0.753

Table B.8. Averaged results of training AUC scores with various values of K

Learning Schedule We examine the performance of ALTBI with respect to the learning rate. We use the Adam optimizer with various learning rates ranging from $1e-4$ to $1e-1$, and the table B.9 compares the averaged AUC on `ADBench` datasets. We observe that when the learning rate is larger than $1e-03$, the performance of the model deteriorates and stabilizes. For this reason, we set the learning rate to $1e-03$ in our experiments.

Learning rate	1e-04	2.5e-04	5e-04	1e-03	2.5e-03	5e-03	1e-02	2.5e-02	5e-02	1e-01
AUC	0.712	0.743	0.756	0.762	0.744	0.738	0.735	0.737	0.739	0.738

Table B.9. Averaged results of training AUC scores with various values of learning rate

Iteration for ensembling within a single model We evaluate the best T_1 and T_2 for ensembling within a single model. We compare three values of T_1 and four values of $T_2 - T_1$, and the table B.10 shows the averaged results on ADBench datasets. We can see that low values of T_1 and T_2 result in lower scores, so we set T_1 to 70 and T_2 to 90.

$T_2 - T_1$	T_1		
	50	60	70
5	0.757	0.760	0.760
10	0.758	0.761	0.760
20	0.759	0.760	0.762
30	0.760	0.762	0.760

Table B.10. Averaged results of training AUC scores with various values of iteration for ensembling

ALTBI for addressing SSOD We compare ALTBI with other methods in SSOD tasks. First, we split inliers into two sets with ratios of 7 : 3 and use the first partition as a training dataset, and regard the rest inliers and outliers as the test dataset.

Table B.4&B.5, and Figure B.1 show the AUC and PRAUC results of the test datasets. We can observe that ALTBI is still competitive in addressing SSOD tasks.

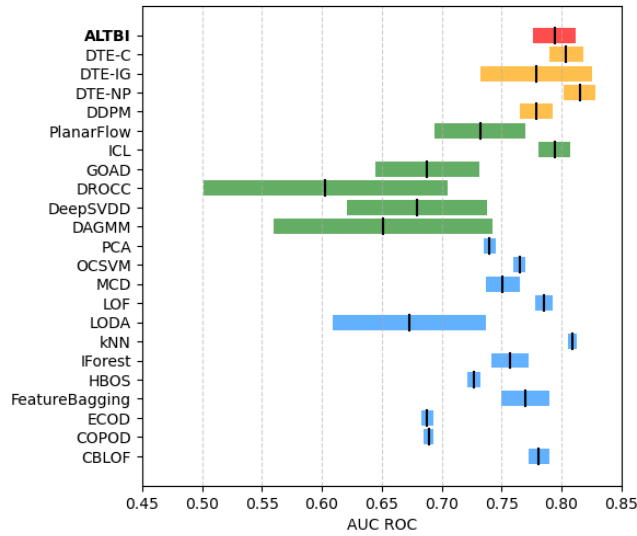


Figure B.1. Test AUC ROC means and standard deviation on the 57 datasets from ADBench over five different seeds in semi-supervised setting. Color scheme: red (IM-based), orange (diffusion-based), green (deep-learning-based), blue (machine-learning-based).

B.5. Further discussions: Robustness of ALTBI in DP

DP-SGD (Abadi et al., 2016) is a variant of SGD used for updating parameters while ensuring differential privacy (DP, Dwork (2006)) for the model. For each sample \mathbf{x} , with its corresponding per-sample loss $\tilde{l}(\theta; \mathbf{x})$, we compute the gradient vector $\nabla_{\theta} l(\theta; \mathbf{x})$. This gradient is then clipped using a specified positive constant $C > 0$ and combined with Gaussian noise drawn from $\mathcal{N}(0, \sigma^2 C^2 I)$ to produce a modified gradient:

$$\nabla_{\theta}^{\text{DP}} \tilde{l}(\theta; \mathbf{x}) = \frac{\nabla_{\theta} \tilde{l}(\theta; \mathbf{x})}{\max\left(1, \frac{\|\nabla_{\theta} \tilde{l}(\theta; \mathbf{x})\|_2}{C}\right)} + \mathcal{N}(0, \sigma^2 C^2 I),$$

where $\sigma > 0$ is another pre-specified constant. In practice, we set $(C, \sigma) = (10, 0.7)$ to carry out DP experiments. The parameters θ is then updated using this modified gradient \tilde{l} with the conventional SGD method or its variants such as Adam (Kingma & Ba, 2014).

For a given loss function to be compatible with DP-SGD, the loss function must be separable across mini-batch samples. However, ALTBI uses a threshold that is calculated based on the current per-sample loss values. Due to this, DP-SGD cannot be directly applied to ALTBI, as the truncated loss function is not separable. This issue can be easily addressed by calculating the threshold using the per-sample loss values from the previous update, i.e., using τ_{t-1} instead of τ_t .

We consider two versions of ALTBI: one that applies mini-batch increment and truncated loss, i.e., $(\gamma, \rho) = (1.03, 0.92)$, and one that does not, i.e., $(\gamma, \rho) = (1.0, 1.0)$. As a measure of DP, we adopt (ϵ, δ) -DP, which is the standard measure to assess differential privacy. With a fixed $\delta = 1 \times 10^{-5}$, we train the models using a DP-SGD algorithm until the privacy budget ϵ does not exceed 10. To implement DP-SGD, we use the `Opacus` library (Yousefpour et al., 2021) in Python.

Similar to the SSOD analysis, we split the entire dataset into two parts with a 7:3 ratio, treating the larger portion as training data and the remaining portion as test data. The test AUC results for 20 tabular datasets are presented in Table B.11. We observe that using mini-batch increment and the truncated loss function results in less degradation in averaged AUC performance (from 0.759 to 0.750) compared to not using these techniques (from 0.729 to 0.651). This indicates that our method provides robustness in performance when applying DP.

Data	$(\gamma, \rho) = (1.03, 0.92)$		$(\gamma, \rho) = (1.0, 1.0)$	
	w/o DP	w/ DP	w/o DP	w/ DP
breastw	0.725	0.981	0.981	0.969
cardio	0.542	0.927	0.802	0.820
cardiotocography	0.803	0.669	0.566	0.623
celeba	0.662	0.809	0.739	0.711
census	0.901	0.569	0.665	0.464
fault	0.923	0.588	0.684	0.557
fraud	0.771	0.928	0.943	0.658
landsat	0.744	0.368	0.519	0.296
magic.gamma	0.806	0.780	0.794	0.722
musk	0.684	0.439	1.000	0.393
optdigits	0.868	0.552	0.629	0.520
pageblocks	0.954	0.790	0.882	0.776
pima	0.760	0.716	0.715	0.683
satimage-2	0.982	0.952	0.998	0.865
skin	0.846	0.889	0.804	0.859
spambase	0.477	0.722	0.545	0.437
speech	0.883	0.581	0.474	0.487
stamps	0.947	0.849	0.876	0.805
wine	0.495	0.914	0.886	0.907
wdbc	0.411	0.559	0.503	0.478
Average	0.759	0.729	0.750	0.651

Table B.11. The average test AUC results for 20 datasets with and without DP applied under the conditions of $\gamma = 1.03, \rho = 0.92$ and $\gamma = 1.0, \rho = 1.0$